Spectrochimica Acta Part B 124 (2016) 25–39

Contents lists available at ScienceDirect

Spectrochimica Acta Part B

journal homepage: www.elsevier.com/locate/sab

Characterization of the large area plane-symmetric low-pressure DC glow discharge

S. Avtaeva [b], V. Gorokhovsky [a,*], S. Myers [a], S. Robertson [c], E. Shunko [d], Z. Zembower [a]

[a] Vapor Technologies, Inc., Longmont, CO, USA
[b] Novosibirsk State University, Novosibirsk, Russia
[c] University of Colorado, Boulder, CO, USA
[d] Superior Twp., MI, USA

ARTICLE INFO

Article history:
Received 10 November 2015
Received in revised form 15 June 2016
Accepted 17 August 2016
Available online 18 August 2016

Keywords:
Glow discharge
OES
Hairpin probe
Langmuir probe

ABSTRACT

Electron density and temperature as well as nitrogen dissociation degree in the low-pressure (10–50 mTorr) large area plane–symmetric DC glow discharge in Ar-N_2 mixtures are studied by probes and spectral methods. Electron density measured by a hairpin probe is in good agreement with that derived from the intensity ratio of the N_2 2nd positive system bands $I_{C,1-3}/I_{C,0-2}$ and from the intensity ratio of argon ions and atom lines I_{ArII}/I_{ArI}, while Langmuir probe data provides slightly higher values of electron density. Electron density in the low-pressure DC glow discharge varies with the discharge conditions in the limits of ~10^8–10^{10} cm^{-3}. The concept of electron temperature can be used in low-pressure glow discharges with reservations. The intensity ratio of (0–0) vibrational bands of N_2 1st negative and 2nd positive systems $I_{391.4}/I_{337.1}$ exhibits the electron temperature of 1.5–2.5 eV when argon fraction in the mixture is higher than nitrogen fraction and this ratio quickly increases with nitrogen fraction up to 10 eV in pure nitrogen. The electron temperature calculated from Langmuir probe *I-V* characteristics assuming a Maxwellian EEDF, gives T_e ~ 0.3–0.4 eV. In-depth analysis of the EEDF using the second derivative of Langmuir probe *I-V* characteristics shows that in a low-pressure glow discharge the EEDF is non-Maxwellian. The EEDF has two populations of electrons: the main background non-Maxwellian population of "cold" electrons with the mean electron energy of ~0.3–0.4 eV and the small Maxwellian population of "hot" electrons with the mean electron energy of ~1.0–2.5 eV. Estimations show that with electron temperature lower than 1 eV the rate of the direct electron impact ionization of N_2 is low and the main mechanism of N_2 ionization becomes most likely Penning and associative ionization. In this case, assumptions of the intensity ratio $I_{N_2^+,391}/I_{N_2,337}$ method are violated.

In the glow discharge, N_2 dissociation degree reaches about 7% with the argon fraction in the Ar-N_2 mixture < 10% and decreases afterwards approaching to ~1–2% when the argon percentage becomes 90% and higher. The atomic nitrogen species is produced by electron-impact processes such as, collisions between electrons and nitrogen molecules or between electrons and N_2^+ ions. At small Ar fraction in Ar-N_2 mixtures, the atomic nitrogen species is most likely produced by the collisions between electrons and N_2^+ ions.

© 2016 Elsevier B.V. All rights reserved.

1. Introduction

Low-pressure plasma technology provides several varieties of applications in the microelectronics industry and materials processing. There has been a recent increase of interest in low-pressure glow discharge (LPGD) plasmas. Among the wide variety of applications utilizing low-pressure discharge plasma there are plasma etching and coating deposition technologies. Both of these technologies are used in several industries such as, semiconductors, optical coatings, flat panel displays, hard coatings for cutting and forming tools, decorative coatings, deposition of diamond and diamond-like films, surface modification by plasma immersion ion implantation and ionitriding, and plasma enhanced magnetron sputtering coating deposition processes [1,2]. The properties of the LPGD operating in pressures ranging from 10 to 100 mTorr are different from conventional glow discharge operating in pressures typically ranging from 1 to 100 Torr and are less studied and understood. Technological and laboratory plasmas are classified by their electron temperature, T_e, and electron density, n_e in addition to densities of other charged and neutral particles [2,3]. There are many different diagnostic techniques used for the measurement of these parameters, the most common of which are electric probes, microwave diagnostics, and optical spectroscopy. In some cases the electron energy distribution function (EEDF) can be obtained from Langmuir probe *I-V* characteristics [4,5].

* Corresponding author.
E-mail address: vgorokhovsky@vaportech.com (V. Gorokhovsky).

http://dx.doi.org/10.1016/j.sab.2016.08.021
0584-8547/© 2016 Elsevier B.V. All rights reserved.

Electrostatic probes represent contact diagnostic techniques. Their usage may influence discharge plasma properties which results in uncontrollable measurement errors in the plasma parameters. The microwave resonator probe, also known as the “hairpin” probe, is a simplified version of microwave (MW) plasma diagnostics that allows the measurement of electron density with high accuracy [6,7]. The operating principles of the hairpin probe are similar to the cavity resonance shift method [8] in which the change of the resonance frequency of a microwave resonator is due to the change of the plasma dielectric properties that are dependent upon electron density. The resonator probe allows measurement of the local plasma density while the cavity resonance method averages the plasma density over the cavity volume.

Optical spectral diagnostic methods are widely used in diagnostics of gas discharges owing to their contactless nature [9–18]. Optical emission spectroscopy (OES) is one of the most widely used diagnostic techniques for low-temperature plasmas. T_e and n_e can be extracted from emission spectra of atomic or molecular species excited by electron-impact processes under certain simplified conditions, for example, the assumption of the Maxwellian EEDF [19,20]. As well, the method of optical actinometry is frequently used to determine the absolute concentrations of species originated in non-equilibrium conditions of low-pressure gas discharges [21–25].

In this paper, the parameters of the glow discharge between large flat electrodes, operating in atmospheres of Ar or Ar-N_2 mixtures in pressures ranging from 10 to 50 mTorr with and without external magnetic fields are obtained by the combination of Langmuir probes, hairpin probes and OES plasma diagnostics techniques. The large area glow discharge at such a low pressure has not been previously studied in a comprehensive collection of diagnostic techniques. The primary goal of this paper is characterization of the composition of the large area glow discharge plasma commonly used in industrial PVD and CVD coatings, plasma cleaning, ionitriding and other surface treatment processes with the emphasis on methodology and its experimental verification. The experimental setup is briefly described in Section 2. Sections 3 and 4 present the Langmuir and microwave probe techniques details and the OES methodology specifics, correspondingly. Section 5 is dedicated to analysis of the low-pressure discharge characteristics obtained by Langmuir and hairpin MW resonance probes as well as by OES to find the electro-physical characteristics including T_e and n_e as well as the electron energy distribution function (EEDF). In addition, Section 5 contains results of N_2 dissociation degree measurements by the optical actinometry method. Effects of discharge conditions such as gas pressure and composition, discharge voltage, and external magnetic field are studied.

2. Experimental setup

The experimental setup is shown in Fig. 1. The large area glow discharge is ignited between a flat plate cathode and the bottom and top parallel walls of a vacuum chamber (grounded anode). The rectangular vacuum chamber is 3 m long and has a cross-section of 20 × 60 cm. The cathode plate was placed in the middle of the vacuum chamber parallel to its walls, keeping the plate-to-wall distance to 11 cm. Two cathode plates made of 304 stainless steel were used in this experiment: “cathode plate 1” has dimensions of 30 × 50 cm and “cathode plate 2” has dimensions of 7 × 50 cm to match the dimensions of the magnetic coils. An MDX-1 power supply manufactured by Advanced Energy Industries, Inc. was used to power the cathode plate. The cathode bias was varied from 600 to 1000 V. The glow discharge was ignited in an Ar-N_2 mixture at gas pressures of 10–50 mTorr. Ar concentration in the mixture was changed from 0% (pure nitrogen) to 100% (pure argon). Langmuir and hairpin probes were placed near the middle point of cathode-anode distance as shown in Fig. 1.

The experiments with cathode plate 1 were conducted without an external magnetic field. When cathode plate 2 was used, two rectangular magnetic coils (65 × 20 cm) with 196 turns of magnetic wire were attached outside of the chamber walls. These coils were used to generate longitudinal magnetic fields along the discharge column if it was required in the experiment. The distance between the coils was 23 cm. Cathode plate 2 was positioned approximately in the middle of the coils.

The magnetic field within the discharge area was controlled by the magnetic coil current and was changed from 0 to 150 G. The actual magnetic field produced by the magnetic coils in the discharge area was compared to FEM calculations generated by COMSOL [26]. The experimental and calculated magnetic field comparison at the midpoint between the coils in an unmatched configuration demonstrates good agreement (Fig. 2, left). The magnetic field map produced by the FEM calculation is shown in Fig. 2, right. The magnetic field is quite uniform across a ~7 cm wide area of cathode plate 2.

The discharge current density, j_c, measured when plate 2 was used as a cathode for all process variables (pressure, discharge voltage, gas composition, and magnetic field) was j_c ~ 0.3 ± 0.05 mA/cm^2.

The low-pressure glow discharge radiation was collected by a collimated lens along a very narrow area parallel to the walls of the chamber that passes in the middle between the cathode plate and one of the chamber walls. The emission was then focused at the fiber optic cable

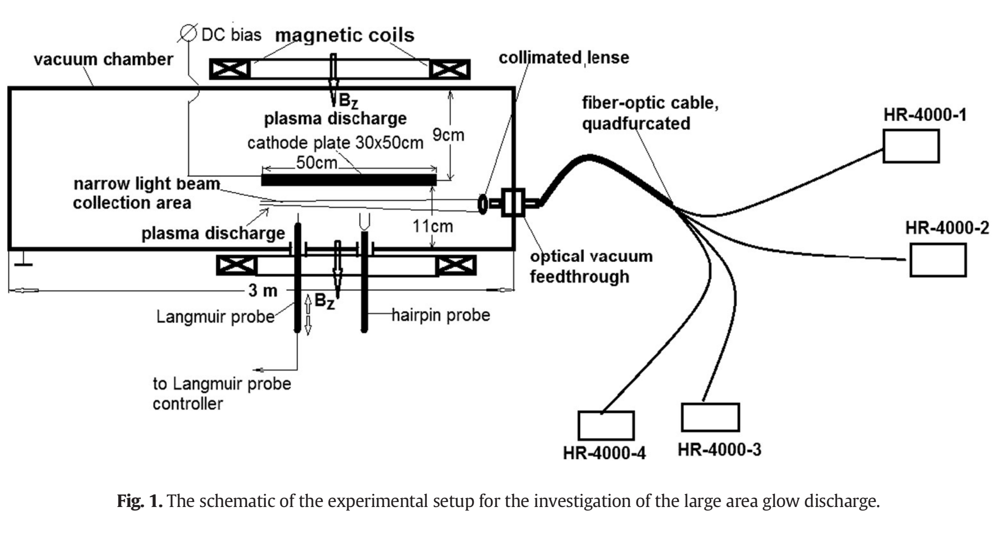

Fig. 1. The schematic of the experimental setup for the investigation of the large area glow discharge.

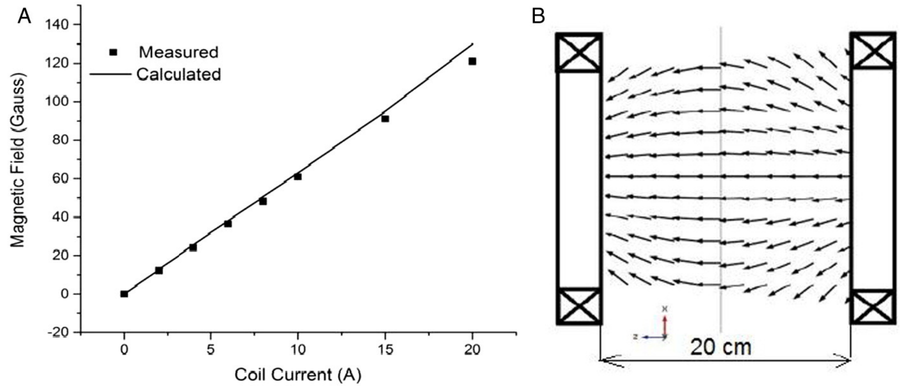

Fig. 2. Comparison of the experimentally measured magnetic field and FEM calculated magnetic field at the midpoint between the electromagnetic coils in an unmatched configuration (left) and the FEM modeling of a magnetic field map between rectangular electromagnetic coils at the total coil current of 1000 amp-turns: 200 turns of magnetic wire with current of 5 A (right).

through an optical vacuum feed through. The fiber optic cable was divided in 4 channels to conduct plasma radiation toward four Ocean Optics spectrometers: HR-4000-1, HR-4000-2, HR-4000-3 and HR-4000-4, with bandwidths of 199–428, 399–613, 600–799 and 800–972 nm, respectively as it is shown in Fig. 1. The devices (with gratings of 1200 L/mm) have optical resolutions of ~0.03 nm and have high sensitivity detectors [27]. Relative sensitivity of the devices as a function of wavelength was calibrated using the DH-2000-CAL having two calibrated light sources in wavelength of 220–1100 nm [27]. The 5 μm wide slits were positioned at the entrance of each spectrometer. A total of five spectra were taken and averaged per scan. The relative standard deviation of the measured intensities of the lines and bands does not exceed 7%.

3. Probe techniques details

3.1. Langmuir probe measurements

The cylindrical Langmuir probe used in this study to measure the electron temperature and electron density as well as the EEDF was manufactured by Hiden Analytics and used a tungsten wire filament 150 μm in diameter with an active length of 10 mm, which was enclosed in an alumina tube. The filament was cleaned prior to each measurement using electron heating by applying a + 100 V potential for 10 s. The measurements were taken by scanning the bias voltage at a rate of 1 V/0.66 s. The Langmuir probe was positioned approximately between the cathode plate and the chamber wall (grounded anode) with the possibility of a linear displacement of ±30 mm. As a rule T_e and n_e in the discharge plasma were calculated from the *I-V* curves generated by the probe by the tangent line method described in detail in [5]. The steps for the calculation are as follows. First, the plasma potential V_p was extracted from the *I-V* curve by the voltage corresponding to the maximum of the derivative d*I*/d*V* of the *I-V* curve, where $\mathrm{d}^2I\,/\,\mathrm{d}V^2 = 0$. Alternatively, V_p was defined graphically as a cross-section of two slopes: below $V = V_p$ and above $V = V_p$ on the ln(I) chart on both sides of its knee-shaped bend of the ln$I$(V) curve [5]. T_e is the slope of the derivative of the semi-logarithmic *I-V* or d(ln*I*)/d*V* on the left side (toward negative voltage) of the knee point of the ln$I$(V) curve or plasma potential V_p. Electron density, n_e was calculated from the electron thermal current at the point where the plasma potential is equal to the probe potential [5]:

$$j_{es} = j_p(V = V_p) = {}^1/_4 n_e q_e \nu_{T_e} \left[A/m^2\right]. \tag{1}$$

Here $j_p(V = V_p)$ is plasma current density to the probe at the probe potential equal to the plasma potential, q_e is charge of electron, and ν_{T_e} is thermal velocity of electrons in plasma in the vicinity of the probe surface:

$$\nu_{T_e} = \sqrt{\frac{q_e T_e}{2\pi m_e}}[\mathrm{m/s}], \tag{2}$$

where T_e is electron temperature and m_e is the mass of an electron.

The electron distribution function can be expressed from the probe *I-V* second derivative as [28]:

$$f\left(\sqrt{2eV/m}\right) = V\frac{4m}{e^2 n S_s} i''(V). \tag{3}$$

This relation was used to obtain the EEDF in the LPGD by double differentiation of the Langmuir probe *I-V* characteristics [29,30].

The array of the probe current first derivatives i'_n over the probe potential V was calculated from the array of experimental points i_n of the probe *I-V* characteristics, where n is a number of the experimental point, and a difference of the probe potentials between any of the neighbor points n and $n + 1$ was a constant value ΔV, by the almost obvious expression.

$$i'_n = [\Delta V N(N-1)]^{-1} \sum_{k=1}^{N} (i_{n+k} - i_{n-N+k}), \tag{4}$$

assuming averaging of the i'_n value over N measurements in the symmetrical vicinity of the point n. And, by analogy, the array of the probe current second derivatives i''_n over the probe potential V was calculated from the array of the probe current first derivatives i'_n by the similar expression

$$i''_n = [\Delta V N(N-1)]^{-1} \sum_{k=1}^{N} (i'_{n+k} - i'_{n-N+k}). \tag{5}$$

The procedure allows one to derive the probe current second derivatives i''_n over the probe potential V with averaging around N experimental points with high accuracy.

Representing average thermal velocity of electrons $\langle v \rangle = \int_0^\infty v f(v) dv$ in the form

$$\langle v \rangle\,[\mathrm{cm/s}] = 5.93 \times 10^7 \int_0^\infty V i''(V) dV \left(\int_0^\infty \sqrt{V} i''(V) dV \right)^{-1} \tag{6}$$

one can calculate the electron density, n_e by the equation.

$$n\left[\mathrm{cm}^{-3}\right] = 0.3973 \times 10^{10} \frac{i(0)\,[\mu A]}{r_z\,[\mu\mathrm{m}]\,l_z\,[\mathrm{cm}]\langle v\rangle \times 10^{-7}[\mathrm{cm/s}]}, \tag{7}$$

where $i(V)$ is the probe *I-V* characteristic, $i(0)$ is the probe current at the point of $V{=}0$, $i''(V)$ is the second derivative with respect to the probe potential V, r_z and l_z are the cylindrical probe radius and its operating length which correspond to the surface area $S_z = 2\pi r_z l_z$.

The plasma potential V_p was defined at the minimum of the derivative $i'(V)$ of the probe current.

3.2. Hairpin MW resonator probe measurements

The principle of measuring electron density by hairpin probe is based on the relative shift of its resonance frequency from its resonance frequency in vacuum. The hairpin probe measures the electron density from the change in the probe resonance frequency [6,7]. Plasmas with low electron density exhibit lower frequencies than plasmas containing higher electron density. For a given hairpin dimensions, the resonance frequency fr only depends on plasma permittivity via $fr = fo\,/\,\varepsilon^{0.5}$; where $fo = c\,/\,4l$ is vacuum resonance frequency of the probe and l is the probe length. In a magnetic field the plasma permittivity perpendicular to the applied B-field can be obtained using [31]

$$\varepsilon_p^{\perp} = 1 - \frac{f_{pe}^2}{f_r^2 - f_{ce}^2}. \tag{8}$$

Here, $f_{ce} = eB\,/\,m_e$ is gyro-frequency of electrons and f_{pe} is electron plasma frequency.

The measurement setup is shown in Fig. 3. This setup consists of two power supplies, a voltage controlled microwave oscillator-crystal, a RF power indicator, a hairpin-shape resonator-probe, and a millivolt meter. The hairpin resonator was fork-shaped and was 75 mm long with a 20 mm gap. The “black box” in the figure contains the voltage controlled oscillator which is powered by a 12VDC supply and scanned by a 0–20 V DC supply, which has a resolution of 0.001 V.

The frequency counter displays the frequency output from the “black box” for the corresponding voltages. When a resonant frequency is achieved, the diode receiver generates a DC voltage which is observed on the millivolt meter. By changing the input voltage while observing the millivolt meter, one can identify a peak voltage which corresponds to the resonance frequency of the probe.

To further automate the process and obtain a temporal resolution of plasma density measurements, an oscilloscope in conjunction with a 0–20 V function generator was added to the setup (Fig. 3b). However, the oscilloscope replaces the millivolt meter and is connected to the function generator, which replaces the 0–20 V power supply. The function generator is set to output a 0–20 V triangle wave for frequencies ranging from 5 Hz to 5 kHz. This setup requires a calibration polynomial to relate the output voltage coming from the function generator and the frequency output from the microwave oscillator-crystal. This is accomplished by changing the frequency every ~100 MHz and recording the corresponding voltage.

With assistance from an oscilloscope, one can determine the peak voltage, from which the frequency can be calculated by means of a calibration curve. This entails the user to observe shifts in resonance frequency, which directly correlates to electron density. The total time range of the hairpin probe oscillogram used in this study is approximately 2 s and has a resolution of 0.2 ms to 10 ms depending on the chosen frequency of the function generator. The distribution of plasma densities per selected duration for each scan at a given plasma condition (pressure, cathode voltage and magnetic field) were then presented in histogram form.

4. OES methodology details

4.1. Electron temperature

Electron temperature was estimated from the corona model using an intensity ratio $R_{391/337}$ of the (0–0) vibrational band of the nitrogen first negative system (391.4 nm) and (0–0) vibrational band of the nitrogen second positive system (337.1 nm). For a low degree of vibrational excitation in plasmas, the populations of the $N_2(C^3\Pi_u, \nu{=}0)$ and $N_2^+(B^2\Sigma_u^+, \nu{=}0)$ excited states are determined by the processes of direct electron-impact excitation from the ground state of nitrogen [32,33].

At low pressures, low ionization degree quenching $N_2(C^3\Pi_u, \nu{=}0)$ in collisions with heavy particles is small. Estimations show that $N_2(B^2\Sigma_u^+, \nu{=}0)$ depopulation frequencies by associative conversion of the nitrogen ions and the charge transfer at collisions with Ar atoms are much less than the frequency of spontaneous radiative depopulation $(\tau_0)^{-1}$. Thus, depopulation of the $N_2(C^3\Pi_u, \nu{=}0)$ and

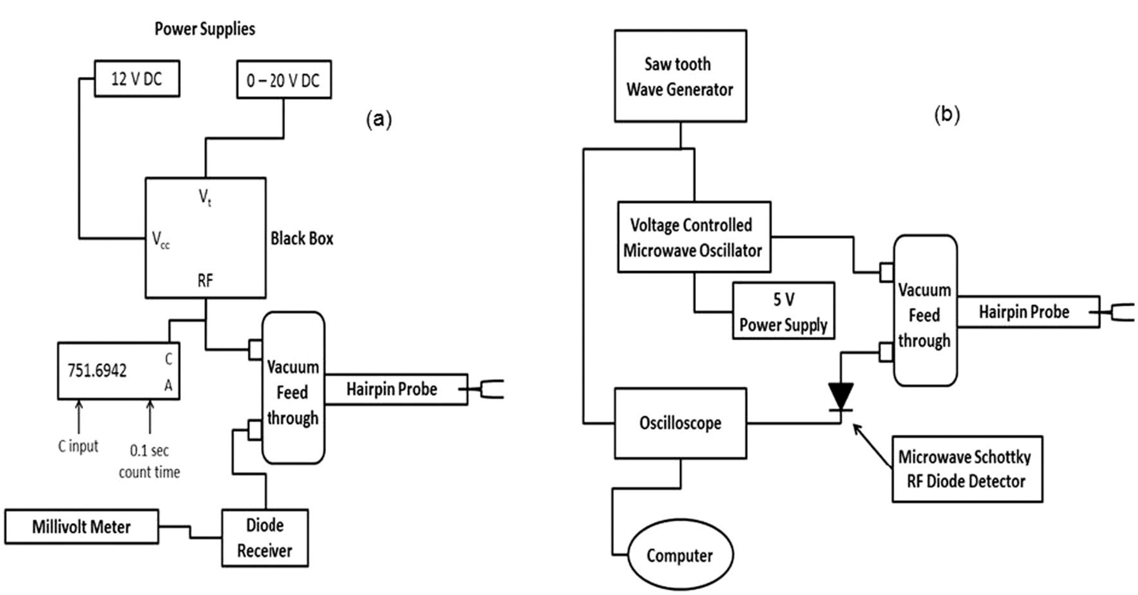

Fig. 3. Measurement schematics with the hairpin probe where (a) is the stationary measurement and (b) is the dynamic measurement.

$N_2^+(B^2\Sigma_u^+, \nu=0)$ occurs due to spontaneous radiative depopulation. In this case, the intensity ratio $R_{391/337}$ can be calculated theoretically. The required intensity ratio is [32,33]

$$R_{391/337} = \frac{I_{N_2^+,391}}{I_{N_2,337}} = \left(\frac{\lambda_{391}}{\lambda_{337}}\right)^{-1} \frac{A_{vib}^{391}}{A_{vib}^{337}} \frac{k_{exc}^{391}}{k_{exc}^{337}}; \tag{9}$$

The excitation rate constants k_{exc} must be defined to complete the ratio shown in (Eq. (9)) and can be calculated knowing the excitation cross-section σ_{exc} and the electron energy distribution function (EEDF), f. Parameters of τ_0 and A_{vib} of the (0–0) vibrational band of the nitrogen first negative system (391.4 nm) and (0–0) vibrational band of the nitrogen second positive system (337.1 nm) we taken from [34] and are presented in the (Table A1). The authors used emission excitation cross sections of the 337.1 nm and 391.4 nm bands at electron collisions with N_2 by Itikawa [35].

4.2. Electron density

Two methods were applied to estimate electron density.

1) The contour graph of population ratio $\frac{n_{C,1}}{n_{C,0}}$ of nitrogen molecules $N_2(C^3\Pi_u, \nu=1)$ and $N_2(C^3\Pi_u, \nu=0)$ as a function of the electron temperature and density, calculated by solving the rate balance equations of $N_2(X^1\Sigma_g^+, \upsilon)$, $N_2(A^3\Sigma_u^+)$, $N_2(B^3\Pi_g)$ and $N_2(C^3\Pi_u)$ excited nitrogen molecules for low-pressure ICP and CCP discharges in nitrogen at 1 Pa (7.5 mTorr) (a nitrogen collisional-radiative model (CRM)) [19,36] were used to derive electron density. The population ratios $\frac{n_{C,1}}{n_{C,0}}$ were calculated from the measured intensity ratio $\frac{I_{C,1-3}}{I_{C,0-2}}$ of nitrogen bands of 2nd positive system. For the second positive system (N_2, $C^3\Pi_u \rightarrow B^3\Pi_g$), the self-absorption processes are ignored since the lower state $N_2(B^3\Pi_g)$ is an excited state and has a very low density. Therefore, the measured intensity ratios $\frac{I_{C,1-3}}{I_{C,0-2}}$ are related to the excited state population ratios $\frac{n_{C,1}}{n_{C,0}}$ by

$$\frac{n_{C,1}}{n_{C,0}} = \frac{I_{C,1-3}}{I_{C,0-2}} \frac{q_{0-2} s_{375}}{q_{1-3} s_{380}}; \tag{10}$$

Here q_{0-2}, q_{1-3} are Franck-Condon factors for transitions $N_2(C^3\Pi_u, \nu') \rightarrow N_2(B^3\Pi_g, \nu'')$ and s_λ is sensitivity of the spectral recorded system at wavelength λ. The Franck-Condon factors of transitions for the (0–2) and (1–3) bands of the second positive system (2^{nd}PS) of N_2 were used from [37] (Table A2 of Appendix A).

It is reasonable to assume that for low-pressure arc discharges at pressures between 2 and 25 mTorr the contour graph of the population ratio $\frac{n_{C,1}}{n_{C,0}}$ is valid as the population of $N_2(C^3\Pi_u, \nu')$ levels is determined by the same processes as in the calculation from Zhu and Pu at 7.5 mTorr [19]. The radial dimensions of these discharges are of the same order as was mentioned in [19]. The authors assume that some small differences in the rates of diffusion and wall process would change the results considerably.

2) In a pure argon glow discharge, we use the intensity ratio of ArII to ArI lines I_{ArII}/I_{ArI} to estimate electron density. In a general gas discharge, the excited Ar ion states can appear in a single-step excitation process (Eq. (11)) as well as in a multi-step excitation process (Eq. (12)).

$$e + Ar \rightarrow (Ar^+)^* + 2e \tag{11}$$

$$e + Ar \rightarrow Ar^+ + 2e; \quad e + Ar^+ \rightarrow (Ar^+)^* + e \tag{12}$$

Bennett et al. [38] provide some quantitative data related to the fractional involvement of single and multi-step excitation processes in the conditions actually encountered in a DC argon ion laser. The discharge data correspond to a filling pressure of 0.2 Torr in a 2-mm capillary at 7 A discharge current. The measurement shows the single-step excitation brings only a small part into excitation of $4p^2D^o{}_{5/2}$ (ArII 487.98) at $T_e \leq 3.5$ eV. At moderate electron temperatures (~1–3 eV) excited argon ions $(Ar^+)^*$ are formed in multi-step excitation (Eq. (12)) as single-step excitation requires more energy. In this case the intensity ratio of an ArII line to an ArI line I_{ArII}/I_{ArI} is first of all a function of the Ar^+ ion density. In pure argon plasma $n_e \approx n_{Ar+}$ and at known T_e electron density n_e can be estimated by I_{ArII}/I_{ArI} ratio.

Considering the single-step Ar^* excitation $e + Ar \rightarrow Ar^* + e$ and the multi-step $(Ar^+)^*$ excitation (Eq. (12)) and depopulation of the excited states by radiation one can get balance equations for argon atoms

$$n_a n_e k_{ex}^a = n_a^* / \tau_a \tag{13a}$$

and for argon ions.

$$n_i n_e k_{ex}^i = n_i^* / \tau_i \tag{13b}$$

Here n_e is electron density, n_a and n_i are densities of argon atoms and ions in their ground states; n_a^* and n_i^* are densities of argon atoms and ions in considered excited states; τ_a and τ_i are life times of the excited states; and k_{ex}^a and k_{ex}^i are excitation rate constants.

Intensities of spectral lines and densities of atoms and ions in excited states satisfy the following ratio $I = \frac{hc}{\lambda_{ki}} n^* A_{ki} l$; where A_{ki} is transition probability, λ_{ki} is wavelength, h and c are Plank constant and light velocity and l is thickness of plasma in the measured direction, respectively [39].

Taking into account these relations and the device sensitivity, the density ratio of argon ions and atoms is

$$\frac{n_i}{n_a} = \frac{k_{ex}^a \tau_a A_{ki}^a \lambda_i}{k_{ex}^i \tau_i A_{ki}^i \lambda_a} \frac{I_i s_{750}}{I_a s_{487}}. \tag{14}$$

Hence,

$$n_e \approx n_i = \frac{k_{ex}^a \tau_a A_{ki}^a \lambda_i}{k_{ex}^i \tau_i A_{ki}^i \lambda_a} \frac{I_i s_{750}}{I_a s_{487}} n_a \tag{15}$$

Here s_λ is sensitivity of the spectral recorded system at wavelength λ.

The ArII 487.98 and ArI750.49 nm lines were chosen to determine n_e. Spectroscopic parameters of these lines are used from [40,41] and are presented in Appendix A (Table A3).

The Van Regemorter formula was used to calculate the excitation rate constant for argon ions k_{ex}^i [42,43]. The excitation rate constant for argon atoms was obtained by integrating the cross section [44] over an assumed Maxwellian distribution under measured value of T_e.

4.3. Optical actinometry for determination of N density in argon-nitrogen discharge

In [17,18], it is shown that in argon-nitrogen discharge at low pressure emission intensity due to a transition from an excited level $[N^*(3p^4S)]$ to a lower state $[N^*(3s^4P)]$ can be expressed as

$$I(N*) = K_N h\nu_N A_N \tau_N n_e [N] k_N^{dir} (1 + s_N), \tag{16}$$

where n_e is electron density, [N] are density of nitrogen atoms in the ground state; τ_N are life time of the excited states; k_N^{dir} are rate constant of direct excitation by electron impact, A_N is transition probability, ν_N is frequency of the transition, h is Plank constant, K_N is a factor, depending on the plasma volume, solid angle, and spectral response of the spectrometer, and s_N is the correction factor accounting for various contribution to the formation of excited nitrogen atoms rather than the direct excitation by electron impact.

Similarly the emission intensity from an excited Ar atom can be written as

$$I(\mathrm{Ar}*) = K_{Ar} h\nu_{Ar} A_{Ar} \tau_{Ar} n_e [\mathrm{Ar}] k_{Ar}^{dir} (1 + s_{Ar}), \tag{17}$$

where s_{Ar} is the correction factor accounting for the excitation from the metastable Ar.

From Eqs. (16) and (17).

$$\frac{[\mathrm{N}]}{[\mathrm{Ar}]} = \frac{I_N}{I_{Ar}} \frac{(1+s_{Ar})}{(1+s_N)} \frac{K_{Ar}}{K_N} \frac{\lambda_N}{\lambda_{Ar}} \frac{A_{Ar}}{A_N} \frac{k_{Ar}^{dir}}{k_N^{dir}} \frac{\tau_{Ar}}{\tau_N}. \tag{18}$$

In [17] it is shown, that with varying Ar content, the s_{Ar} factor does not exhibit a big change because both $[\mathrm{N_m}]$ and $[\mathrm{Ar_m}]$ are counter variant quantities. The s_N factor increases with Ar content but the effect of s_N is also not significant due to small values of $[\mathrm{Ar_m}]$. Therefore, the actinometric relation, Eq. (18), can be used to give a rough estimation of [N] even for the high Ar content discharge [17].

Estimating that in the glow discharge densities of metastable N and Ar atoms are not large due to very low pressure and so factors s_N and s_{Ar} are small in comparison with 1, N density is written as

$$[\mathrm{N}] \approx \frac{I_N}{I_{Ar}} \frac{K_{Ar}}{K_N} \frac{\lambda_N}{\lambda_{Ar}} \frac{A_{Ar}}{A_N} \frac{k_{Ar}^{dir}}{k_N^{dir}} \frac{\tau_{Ar}}{\tau_N} [\mathrm{Ar}] = const \frac{I_N}{I_{Ar}} \frac{k_{Ar}^{dir}}{k_N^{dir}} \frac{x_{Ar}}{x_{N2}} [\mathrm{N_2}], \tag{19}$$

where $const = \frac{K_{Ar}}{K_N} \frac{\lambda_N}{\lambda_{Ar}} \frac{A_{Ar}}{A_N} \frac{\tau_{Ar}}{\tau_N}$, and x_{Ar}, x_{N2} and $[\mathrm{N_2}]$ are the percentage of argon and nitrogen in the gas mixture with the discharge off and the input number density of nitrogen molecules, respectively.

The dissociation degree α is ratio of dissociated molecules $[\mathrm{N_2}]_{diss}$ to nitrogen molecules in the gas mixture with the discharge off $[\mathrm{N_2}]$. So we can write

$$\alpha = \frac{[\mathrm{N_2}]_{diss}}{[\mathrm{N_2}]} 100\% = \frac{[\mathrm{N}]/2}{[\mathrm{N_2}]} 100\%. \tag{20}$$

From Eqs. (18) and (19)

$$[\alpha] \approx const \frac{1}{2} \frac{I_N}{I_{Ar}} \frac{k_{Ar}^{dir}}{k_N^{dir}} \frac{x_{Ar}}{x_{N2}} 100\%. \tag{21}$$

However, quantitatively accurate results can only be obtained if excitations via dissociative channels, the Penning effect, and the quenching of excited states are accounted for.

When the N_2 dissociation degree α is calculated it is easy to find N density as $\mathrm{N} = \frac{2}{100} \alpha \cdot [\mathrm{N_2}]$.

To calculate the excitation rate constant of Ar levels the Maxwell's EEDF experimental cross sections from [44] are used. For rate constants of electron impact direct excitation of 3p levels of nitrogen atoms the expression by Gudmundsson [45] are used:

$$k_N^{dir} = 2.26 \cdot 10^{-14} T_e^{-0.187} \exp(-12.02/T_e), \quad \mathrm{m^3/s}. \tag{22}$$

Monitoring the nitrogen dissociation degree in accordance with Eq. (21) were carried out using two ratios of the spectral lines of nitrogen NI, and argon ArI atoms: $I_{\mathrm{NI},868.03}/I_{\mathrm{ArI},852.14}$ and $I_{\mathrm{NI},862.92}/I_{\mathrm{ArI},852.14}$. Atomic constants of the ArI and NI spectral lines summarized in Table A4 of Appendix A are used from [41,46–49]. The Gudmundsson's rate constant for $2s^2p^33p$ levels of Ar was multiplied by the ratio of statistical weight of a top level of the transition to the total statistical weight of $2s^2p^33p$ levels $g_k/\sum_i g_i$.

5. Results and discussion

To estimate electron density in the LPGD in pure argon Langmuir and hairpin probes and the intensity ratio $I_{\mathrm{ArII}}/I_{\mathrm{ArI}}$ of ArII 487.98 and ArI 750.49 nm lines were used. In the LPGD in Ar-N_2 mixtures the counter graph of the population ratio $\frac{n_{C,1}}{n_{C,0}}$ calculated by the nitrogen band intensity ratio $\frac{I_{C,1-3}}{I_{C,0-2}}$ were used for electron density estimation by OES. The Langmuir probe data exhibit higher electron density values than the data measured by the hairpin probe and OES, which conversely, are quite comparable to each other. It is known, the hairpin MW resonance probe represents a simplified version of MW plasma diagnostics and allows measurement of electron density with high accuracy unlike Langmuir probe analysis which has a high probability to influence discharge plasma properties and may negatively affect results [28]. On the other hand, the Langmuir probe allows more local measurements than the hairpin MW resonance probe and OES.

Electron temperature was measured using the intensity ratio $I_{N_2^+,391}/I_{N_2,337}$ and by the Langmuir probe. The intensity ratio provides an electron temperature of ~1.5–3 eV and higher. Langmuir probe measurements show lower electron temperatures of ~0.2–0.3 eV (Figs. 4 and 5). This discrepancy appears because of non-Maxwellian behavior of the EEDF in the glow discharge as described in Section 5.3 (Tables 1, 2). Two distinct population groups of electrons in the EEDF is observed using double differentiation of the Langmuir probe *I-V* characteristics: the main group of 'thermalized' electrons exhibits a mean electron energy of ~0.3–0.4 eV and the second small group of 'energetic' electrons exhibits a mean electron energy of ~1.0–2.5 eV. The 'energetic' electron population at 2 eV may consist of secondary electrons originating at the walls [50]. T_e determined by the slope of the derivative of the *I-V* semi-logarithmic characteristic reflects the mean energy of the main group of 'thermalized' electrons. At the same time the OES methods show electron temperatures that correspond to 'energetic' electrons since only enough hot electrons can excite the $N_2(C^3\Pi_u)$ and $N_2^+(B^2\Sigma_u^+)$ levels. In addition in the LPGD in Ar-N_2 mixtures the dissociation degree was evaluated using optical actinometry method: by intensity ratio of NI, 862.9/868.0 nm and ArI, 852.1 nm lines.

5.1. Spectra of the low-pressure glow discharge

Fig. 4 shows spectra of the low-pressure glow discharge in Ar, N_2 and their mixtures at a pressure of 34 mTorr, where all strong line and bands are clearly seen and the noise level is weak. Intensities of the discharge spectra are weak. Noise level in the spectra increases as pressure decreases.

In spectra, the authors obtain ArI, ArII and NI lines and N_2 and N_2^+ bands. Intensities of the lines and bands strongly depend on discharge conditions such as, gas composition, pressure, discharge voltage, and magnetic field.

Strong ArI lines corresponding to 2p → 1s transitions (in Pashen's notation) are easily observed in a wavelength range of 690–980 nm in spectra of the LPGD in pure argon and in Ar-N_2 mixtures (Fig. 4d). ArI lines emitted from higher levels are weak. ArII lines are much weaker than ArI lines and are mostly in wavelength range of 450–500 nm (for example, Fig.4e). NI lines are very weak in spectra of the LPGD in pure nitrogen and in Ar-N_2 mixtures and are superimposed by bands of the 1st positive system of nitrogen which lie in the wavelength range of 650–960 nm (Fig.4b). Intensities of NI lines and 1st positive system bands of N_2 decrease promptly when the Ar percentage in Ar-N_2 mixtures grows. Only a few strong bands of 2nd positive system of nitrogen and few strong bands of 1st negative system of N_2^+ ions are observed in spectra of the LPGD at a wavelength range of 300–400 nm and 385–525 nm, respectively (Fig. 4c and a). Argon content in Ar-N_2 mixtures negatively affects the intensity of 1st negative system bands much more than 2nd positive system bands. Three reasons can lead to the effect: 1) a contribution of Penning and associative ionization in N_2

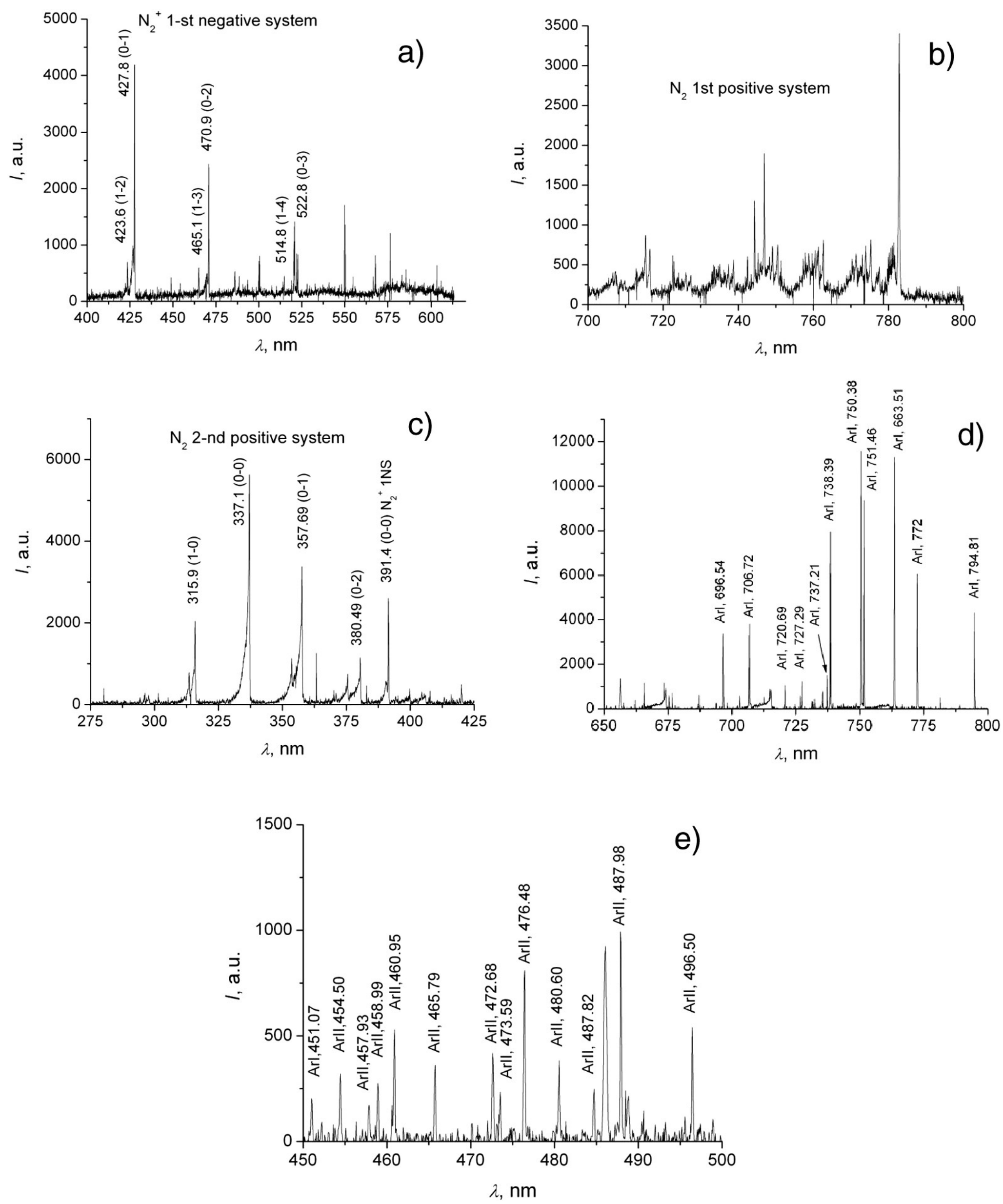

Fig. 4. Spectra of the low-pressure glow discharge at a gas pressure of 34 mTorr and a discharge voltage of 700 V; a, b – pure N_2, c, d – Ar-N_2 (1:1), and e – pure Ar.

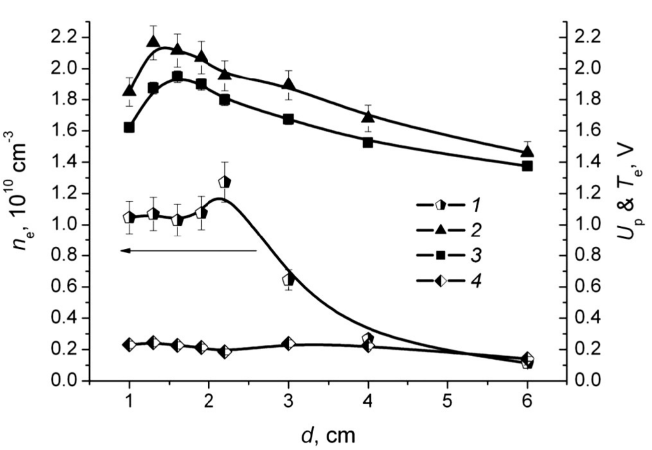

Fig. 5. Distribution of argon plasma parameters within the gap between the cathode and opposite chamber wall (grounded anode) at $P = 25$ mTorr and $U = 1000$ V; *1* – n_e, *2* – U_p via inflection point, *3* – U_p via derivative and *4* – T_e.

ionization mechanism, 2) charge transfer at collisions N_2^+ ions with Ar atoms, 3) population of $N_2(C^3\Pi_u)$ state at collisions of N_2 molecules with metastable argon atoms (Ar_m^*). The first two mechanisms contribute prompt decreasing of the $N_2^+(B^2\Sigma_u^+)$ density when the argon content grows, and the third mechanism hinders decreasing $N_2(C^3\Pi_u)$ density. More detail of the effects of the processes is discussed in Section 5.4.4.

5.2. Spatial distributions of the low-pressure glow discharge parameters

While observing the discharge emission with the naked eye it was found out that the low-pressure glow discharge is stable over time and any visible glow pulsations are not detected. The glow is uniform in a direction along the cathode plate. In the transverse direction, along the discharge gap, increase in glow near the cathode plate can be seen clearly.

Spatial distributions of the glow discharge parameters were estimated from Langmuir probe measurements. The distribution of electron temperature, T_e, electron density, n_e and plasma potential, V_p within

Table 1
Electron parameters in a glow-discharge Ar plasma at $p = 25$ mTorr. Designations: ε_p – energy corresponding to the most probable velocity, $\langle\varepsilon\rangle$ – mean energy, n – electron concentration, λ_D – Debye length, λ_{Te} – free path, ν – collision frequency, V_p – plasma potential.

Electron population	ε_p, eV	$\langle\varepsilon\rangle$, eV	n, 10^{10} cm^{-3}	λ_D, μm	λ_{Te}, cm	ν, 10^7 s^{-1}	V_p, V
Low-energy electrons	0.424 ± 0.170	0.393 ± 0.093	0.194 ± 0.051	110 ± 26	32.3 ± 3.4	0.112 ± 0.008	1.541 ± 0.058
High-energy Maxwellian electrons	0.676 ± 0.127	1.01 ± 0.19	0.040 ± 0.011	314 ± 65	12.7 ± 3.0	0.453 ± 0.133	

the inter-electrode gap between the cathode plate and the opposite chamber wall are shown in Fig. 5 for pure argon at the pressure of 25 mTorr and cathode voltage 1000 V. The characteristic electric field along the discharge column is approximately $E \sim 0.1$ V/cm. The peak in plasma potential at distance of 1.5 cm from cathode plate likely indicates a soft boundary of the cathode fall area and the peak at distance of 2.2 cm probably indicates a soft boundary of the Faraday dark space area. One can see, near the cathode plate in the cathode fall area there is high enough electron density $1 \cdot 10^{10}$ cm^3. The electron temperature is low ~0.2 eV and its variations near the cathode plate are small, however at a distance of 6 cm from the cathode plate it falls to 0.15 eV. The relative standard deviation (RSD) of the T_e measurements is 5–10%.

Shown in Fig. 6 are plasma parameters in Ar-N_2 mixtures as a function of nitrogen partial pressure with a total gas pressure of 25 mTorr and a cathode voltage of 1000 V in the midpoint between the cathode and the chamber wall (the probe tip was placed at distance of $d =$ 5 cm from the cathode plate). The plasma potential slightly decreases when the nitrogen pressure increases, which is attributed to the increase in plasma conductivity. At a nitrogen partial pressure of 2 mTorr in the Ar-N_2 mixtures at total pressure of 25 mTorr the electron temperature T_e reaches its maximum and the electron density n_e reaches its minimum. This is attributed to competition between ionization and recombination processes depended on the mixture composition.

5.3. Electron energy distribution in the glow discharge plasma

It is known that in traditional glow discharges excited at pressures of several Torr and several tens/hundreds of Torr, the EEDF is non-Maxwellian [51,52]. Therefore, one expects that the EEDF in the LPGD is also in a non-equilibrium state.

One important aspect from the data collected in this study is that under pressures of 10–50 mTorr the electron free path is about the same as the discharge gap. For example, the electron mean free path calculated with a total cross section of the electrons scattered on Ar atoms at a pressure of 25 mTorr is 25.7 ± 3 cm. This is twice as long as the discharge gap of approximately 10 cm between the cathode and the anode surfaces, e.g. $\lambda_{T_e} \gtrsim \Delta x$. In the Ar-$N_2$ mixture under 25 mTorr (2.27 mTorr of Ar and 22.7 mTorr of N_2) the electron mean free path 4.7 ± 0.2 cm is about two times less than the gap, e.g. $\lambda_{T_e} \lesssim \Delta x$. In both cases, one can expect in plasma, a spherically symmetric electron velocity distribution function (EVDF) $\boldsymbol{f}(\boldsymbol{v})$ formed by electrons which are accelerated in the electrical field and are scattered by neutral atoms and molecules defining their average thermal velocity.

Fig. 7a displays an *I-V* characteristic obtained for the LPGD plasma in pure Ar under a pressure of 25 mTorr by using the cylindrical Langmuir probe, where $i(V)$ is averaged over 10 scans taken by the Hiden Analytical electronic block. In addition, Fig. 7a shows the first $i'(V)$, and second $i''(V)$ derivatives obtained from the probe's *I-V* characteristic by numerical differentiation using the Savitzky-Golay filtering. The probe tip was immersed in a glow discharge plasma approximately between the cathode plate 1 and the chamber wall (grounded anode). The total voltage drop across the discharge gap was 1000 V and the total discharge current was 0.125 A. On the second $i''(V)$ derivative of the probe's *I-V* characteristic certain periodic oscillations were observed (as shown in Fig. 7a) in the range of $0.65 \lesssim V \lesssim 1.65$ V with a period of $\Delta V =$ 0.31 ± 0.01 V ($\tau = 0.206 \pm 0.006$ s), which can be represented approximately in the following form

$$i''_{\sim}(V) = i''_0 \sin\left(\left(\frac{2\pi}{\Delta\nu}\right)V + \gamma\right), \tag{23}$$

where the amplitude i''_0 and the phase γ are found by their variations that provide the best fitting of the experimental points for the curve defined by Eq. (23). The plasma potential V_p was defined at the minimum of the derivative $i'(V)$ of the first probe current as illustrated in Fig. 7a. Fig. 7b displays the difference $i''(V) - i''_{\sim}(V)$ assuming an elimination of periodic oscillations from the probe signal. This elimination allows one to recognize two regions in the EEDF shape determined by two distinct plasma electron populations: the greater population characterized by the probe signal labeled '0', and the small population labeled '2'. Note here that the presence of insignificant periodic (Fig. 7a) and even smaller non-cyclic (Fig. 7c) noises, which could be observed only on the second derivative of the probe *I-V* characteristic, did not add noticeable changes in the results of the probe *I-V* characteristics processing (see [53]). Moreover, these noises can be clearly recognized on the second derivative of the probe *I-V* characteristic and eliminated mathematically as is shown in Fig. 7a–d by selecting the proper duration of the analyzing saw-tooth voltage.

The oscillations highlight some weak fluctuations existing in the low-pressure glow discharge in spite of apparent uniformity. The nature of the effect is not studied yet, most likely the oscillations are generated by small spatially periodic striation-like components of electric field. It is well-known, in the glow discharges various ionization waves spread, which are determined by transport phenomena, ionization processes and electron kinetics [54].

Fig. 7c displays the portion of the second $i''(V)$ derivative responsible for small electron population and its average behavior which implies a possibility to interpret the section as an exponent (curve 3 in Fig. 7c) which is presumably Maxwellian. Thus, it has an electron distribution function with an electron temperature of $kT = 0.75 \pm 0.06$ eV (mean electron energy $\langle\varepsilon\rangle = (3/2)kT = 1.13 \pm 0.09$ eV) and a population concentration of $n_2 = (2.7 \pm 0.2) \cdot 10^8$ cm^{-3}. After subtracting the value $i''_2 = 5.76 \times 10^{-5} e^{(V/0.75)}$, which is the best polynomial fit of the experimental data points plotted in Fig. 7c (labeled '3' in the Figure), one can obtain a part of the second derivative $i''(V) - i_{\sim}''(V) - i''_2(V)$ which presumably corresponds to the greater electron population. This population is spherically-symmetric and is almost isotropic (shown in Fig. 7d).

Table 1 lists data, which were collected using the same conditions of Ar LPGD plasma mentioned above after being averaged per ten measurements.

Table 2
Parameters of electrons in glow-discharge plasma of mixture 2.27 mTorr of Ar and 22.7 mTorr of N_2. Designations are the same as in Table 1.

Electron population	ε_p, eV	$\langle\varepsilon\rangle$, eV	n, 10^{10} cm^{-3}	λ_D, μm	λ_{Te}, cm	ν, 10^7 s^{-1}	V_p, V
Low-energy electrons	0.251 ± 0.024	0.295 ± 0.050	0.139 ± 0.051	352 ± 19	1.62 ± 0.02	0.75 ± 0.06	1.656 ± 0.025
High-energy Maxwellian electrons	1.63 ± 0.35	2.45 ± 0.53	0.074 ± 0.023	314 ± 65	12.7 ± 3.0	5.25 ± 0.53	

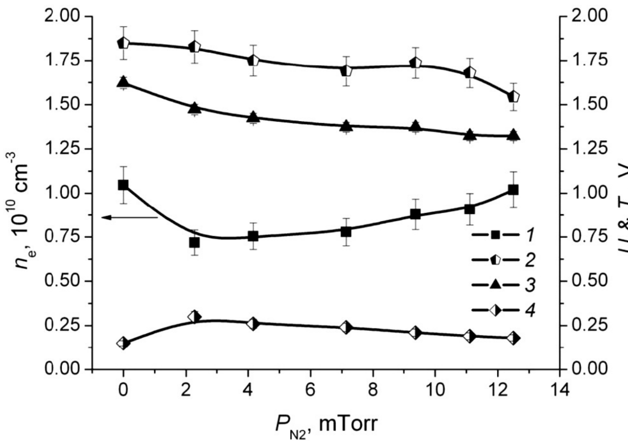

Fig. 6. Plasma parameters at distance of 5 cm from the cathode plate as a function of nitrogen partial pressure in Ar-N_2 mixtures at total pressure 25 mTorr; *1* – n_e, *2* – U_p via inflection point, *3* – U_p via derivative and *4* – T_e.

Two electron populations drifting along the electric field E of discharge is distinguished by two couple of average drift υ_d and thermal $\langle \upsilon \rangle$ velocities: (i) $\upsilon_d = 1.4 \cdot 10^6$ cm/s at $\langle \upsilon \rangle = 3.4 \cdot 10^7$ cm/s, in the case of low-energy electrons corresponding to Table 1, and (ii) $\upsilon_d = 1.66 \cdot 10^6$ cm/s at $\langle \upsilon \rangle = 3.11 \cdot 10^7$ cm/s, in the case of electrons with larger energies corresponding to high-energy Maxwellian electrons in Table 1. If the average drift velocity υ_d of the electrons is negligibly less than their average chaotic velocity $\langle \upsilon \rangle$, $\upsilon_d \ll \langle \upsilon \rangle$, the electron distribution function does not have a dominant direction, that making it almost spherically symmetric and isotropic when the free path of the electrons is comparable to the interelectrode gap.

Table 2 lists the same data as in Table 1 for the LPGD in Ar-N_2 mixture (1:10) also under pressure 25 mTorr and voltage drop 1000 V averaged per ten measurements.

Thus, in the low-pressure glow discharge, the EEDF is non-Maxwellian. The EEDF has at least two populations of electrons: the main cold non-Maxwellian population exhibits a mean electron energy of ~0.3–0.4 eV and the second small Maxwellian population of "energetic" electrons exhibits a mean electron energy of ~1.0–2.5 eV (as shown in Tables 1,2). Furthermore, the presence of the electron population with the mean energy of the electrons $\langle \varepsilon \rangle \sim 1$ eV is corroborated by a relatively high positive plasma potential, $V_p = 1.55$ V, measured by the probe and verified independently by spectral measurements of the plasma radiation, while the presence of the population of the cold electrons shown in Fig. 7d can be explained by a secondary emission from the electrodes and chamber walls under conditions of plasma UV radiation [50].

Two distinct population groups of electrons which have non-Maxwellian EEDF, were also observed by Gamez et al. [51] in argon DC planar-diode glow discharge with argon pressures of 1–3 Torr and discharge currents of 2.5–65 mA using Thomson scattering. Authors stated that using a bi-Maxwellian distribution resulted in a good estimation of the energies of the different electron groups in the discharge. They found one group of 'thermalized' electrons exhibited temperatures of ~0.3 eV and the other group of 'energetic' electrons exhibited temperatures of ~1–1.5 eV and the group of 'energetic' electrons became weaker as the distance from the cathode increases until ultimately disappearing, reaching zero concentration. The non-Maxwellian behavior of the EEDF in the glow discharge was also shown in [55–57]. Gamez et al. [51] consider that the temperatures of the high-energy group of electrons range from 2 to 10 eV and they correspond to gas-phase ionized electrons which were previously involved in collisions as electrons that arise from gas-phase ionization events [56]. In addition, the data presented in [51], show non-Maxwellian behavior of the EEDF in a glow discharge with two distinct groups of electrons with close energies. However, it is surprising that plentiful 'cold' electrons in the low-

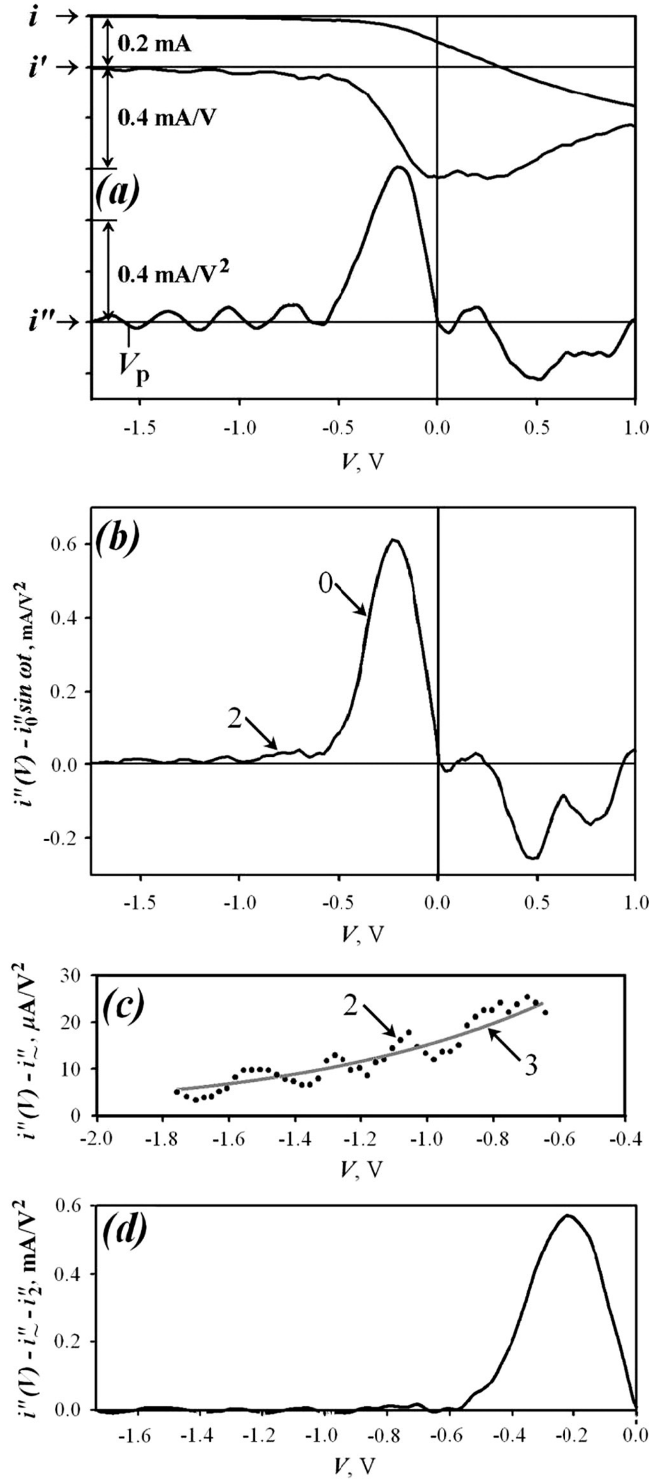

Fig. 7. (a) The *I-V* characteristic of the Hiden Analitics Langmuir probe, $i(V)$, and the first, $i'(V)$, and second, $i''(V)$, derivatives; (b) the second derivative, $i''(V)$ after subtraction of periodic plasma oscillations, 0 – main part, exponential wing; (c) exponential wing of the EEDF determined by presumably Maxwellian "high-energy" electron population, 2 – experiment, 3 – exponential fit; (d) part of $i''(V)$ determined by "low-energy" electron population.

pressure glow discharge also have non-Maxwellian EEDF. Note: the argon discharge pressure used in the work presented here is one order of magnitude lower than in [51]. This decrease in gas pressure results in the reduction of electron collisions and, consequently, complete thermalization of electrons becomes more difficult.

Furthermore, it should be noted that electrons with energies above the threshold for inelastic collisions are particularly important for the glow discharge as they give rise to excitation, ionization, and are therefore important for sustaining of the discharge. These energetic electrons were, however, not observed in the experiments because their fraction is quite low compared to the thermal electrons and the sensitivity of the experiments is not adequate enough to observe them [52].

5.4. The low-pressure glow discharge plasma properties

5.4.1. Voltage effect on electron density

Electron density in the low-pressure glow discharge increases with discharge voltage. Fig. 8 shows the electron density in the glow discharge in pure argon as a function of voltage at argon pressure of 25 mTorr measured by the hairpin probe.

Intensities of NI, ArI, and ArII lines and N_2 and N_2^+ bands emitted by the low-pressure glow discharge in Ar-N_2 mixtures increase with discharge voltage, which is because the increase in electron density. For the LPGD in 0.7Ar-0.3N_2 mixture at pressure 25 mTorr and voltage 900–1000 V the excited state population ratio $\frac{n_{C,1}}{n_{C,0}}$ provides electron density values $8 \cdot 10^8$–$1 \cdot 10^{10}$ cm^{-3} close to values measured by the hairpin probe in pure argon. Unfortunately, intensities of C,1 → B,3 (head at 380.49 nm) and C,0 → B,2 (head at 375.54 nm) bands are very weak at discharge voltages lower than 900 V and could not be used for calculation of the $\frac{n_{C,1}}{n_{C,0}}$ ratio at low voltages. The electron temperature measured by the intensity ratio $\frac{I_{N_2^+,391}}{I_{N_2,337}}$ was ~2.5 eV and has little to no dependence on the glow discharge voltage.

5.4.2. Pressure effect on LPGD properties

Fig. 9 shows intensities of ArI and ArII lines in spectra of the LPGD as a function of pressure. Intensities of all lines increase with gas pressure. The electron temperature in the low-pressure glow discharge in a mixture of 0.7Ar-0.3N_2 calculated by the intensity ratio $I_{N_2^+,391}/I_{N_2,337}$, increases from 2.6 to 2.9 eV when gas pressure increases from 9 to 15 mTorr. Fig. 10 shows the electron density measured by Langmuir and hairpin probes and by the I_{ArII}/I_{ArI} ratio as a function of argon pressure.

Both Langmuir and hairpin probes as well as OES data show that n_e increases with argon pressure, but the Langmuir probe data exhibit higher n_e than the hairpin probe data. The OES data show slightly higher electron densities than the hairpin probe data. In argon as well as in nitrogen, glow discharges at gas pressures lower than 25 mTorr exhibit electron density ranges within $n_e \sim 10^9$ cm^{-3}. When the gas pressure reaches 35 mTorr, the electron density begins to increase faster, and consequently, the dependence changes. This change implies that additional ionization processes arise in gas. This phenomenon should be studied in the future.

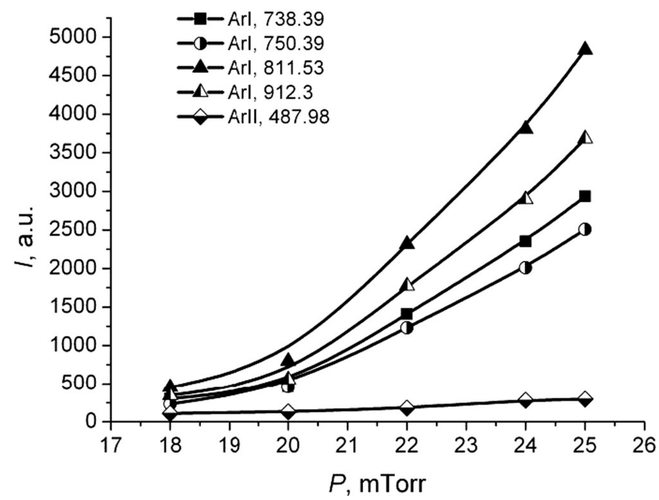

Fig. 9. Intensities of ArI and ArII spectral lines in spectra of the low-pressure glow discharge in pure argon as a function of pressure where the bias is 1000 V.

The Langmuir probe data exhibits higher electron density values than the data measured by the hairpin probe and OES, the n_e measured by OES is a bit higher than the one measured by the hairpin probe. The difference between the Langmuir probe and the hairpin probe measurements increases with growth of pressure. It should be noted, that the Langmuir probe with tip length of 10 mm allows more local measurements than the hairpin probe with resonator length of 75 mm. The main reason for the difference between data of Langmuir and hairpin probes is non-locality of hairpin probe data, the resonator occupies about a half of discharge gap, situated between the wall and the middle point of the discharge gap, therefore the hairpin probe exhibits average data over the discharge part with lower average electron density than in the center of the gap. The increase with pressure in the difference between the n_e measured by the Langmuir and the hairpin probe points to a rise of non-uniformity of discharge parameter distribution over the discharge gap.

5.4.3. Magnetic field effect

The intensities of the ArII 487.98 and ArI 750.49 nm lines and the intensity ratio I_{ArII}/I_{ArI} as functions of a magnetic field in the glow

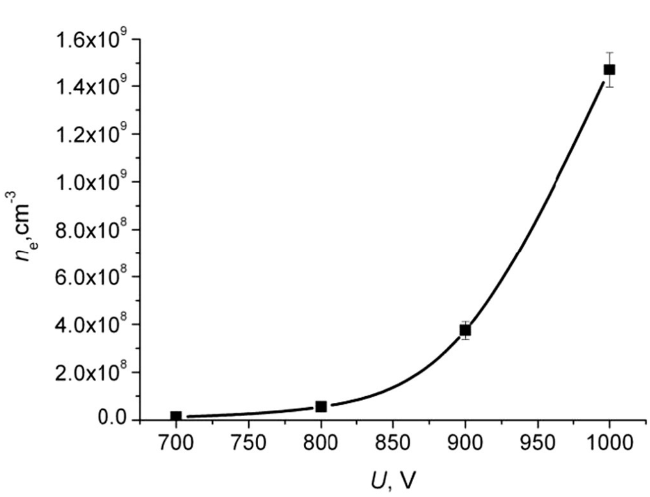

Fig. 8. Electron density measured by the Hairpin probe as a function of voltage in the glow discharge in pure argon at argon pressure 25 mTorr.

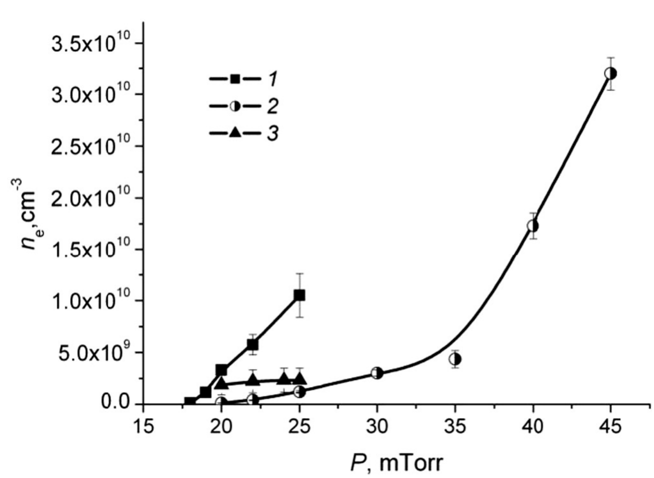

Fig. 10. The electron density in the low-pressure glow discharge in argon as a function of pressure: n_e was measured by Langmuir probe at midpoint of the inter-electrode gap (*1*), by hairpin MW resonance probe (*2*) and by I_{ArII}/I_{ArI} intensity ratio (*3*); $U = 1000$ V.

discharge in longitudinal magnetic field in pure argon are shown in Fig. 11. The electron density estimated by the intensity ratio I_{ArII}/I_{ArI} and measured by the hairpin probe as a function of magnetic field is shown in Fig. 12.

The hairpin probe and OES data show similar values of electron density ~ 10^9–10^{10} cm^{-3}. Both methods reveal that electron density increases with magnetic field and pressure. This behaviors caused by the increase in the number of electron collisions with atoms accompanied by ionization under rise of both pressure and magnetic field. It should be note that increase in magnetic field in some way is similar to increase in pressure because orbital motion of electrons in magnetic field increases number of their collisions with atoms.

As derived from Eq. (8), in a weak magnetic field, when $f_{ce} \ll f_r$, the magnetic field has a negligible effect on hairpin probe measurements. In the range of magnetic field of 25–150 G the gyro-frequency of electrons changes in the range of $0.67 \cdot 10^8$–$4 \cdot 10^8$ Hz. The vacuum resonance frequency of probe $fo = c / 4l$ at the hairpin resonator length of 7.5 cm is $1 \cdot 10^9$ Hz. In the low-pressure glow discharge the hairpin probe resonance frequency $f_r > f_0 \gg f_{ce}$ and the effect of magnetic field on hairpin probe measurements is small. On the other hand, the intensities of ion lines in optical emission spectra of LPGD plasma in a weak magnetic field were low, which increases the deviations of spectral lines intensities up to 10–20%. Moreover, the EEDF in the LPGD is non-Maxwellian and the Van Regemorter formula for the excitation rate constant is only an approximation. Nevertheless, the data from OES and hairpin probe (HP) measurements exhibit reasonable agreement with each other.

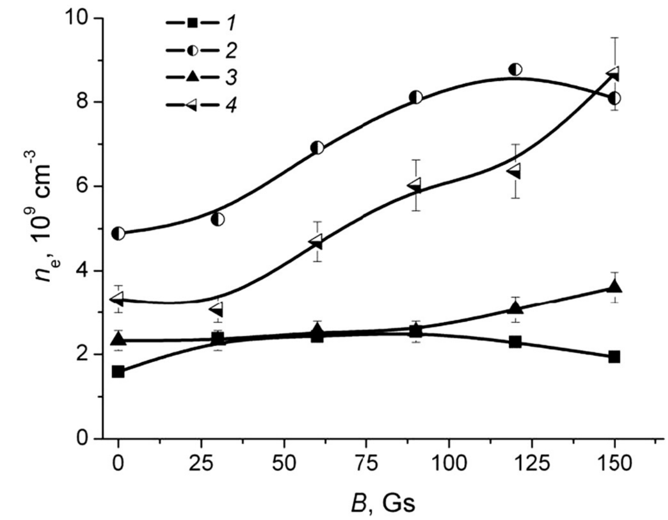

Fig. 12. Electron density, n_e in the glow discharge in the longitudinal magnetic field as a function of the magnetic field; *1*, *2* - OES by I_{ArII}/I_{ArI} intensity ratio and *3*, *4* - MW resonance hairpin probe; *1*, *3* - 30 mTorr and *2*, *4* - 40 mTorr.

5.4.4. Ar concentration effect on characteristics of the low-pressure glow discharge in Ar-N_2 mixtures

Fig. 13 shows head intensities of the (0–0) band of the N_2 second positive system (SPS) and (0–0) band of the N_2^+ first negative system (FNS) (a) and the electron temperature measured by the intensity ratio $I_{N_2^+,391}/I_{N_2,337}$ (b) in the Ar-N_2 low-pressure glow discharge as a function of the Ar fraction in Ar-N_2 mixtures.

One can see the intensity of the (0–0) band of the N_2^+ FNS (391.4 nm) has a maximum at an Ar fraction of 7% in the Ar-N_2 mixture and decreases above 7% whereas, the intensity of the (0–0) band of the N_2 SPS (337.1 nm) reaches a maximum with an Ar fraction of 60–70% in the mixture (Fig. 13a). The electron temperature determined by the intensity ratio $I_{N_2^+,391}/I_{N_2,337}$ at nitrogen fraction in an Ar-N_2 mixture < 50% slow increases from 1.5 to 2.5 eV when the nitrogen fraction in the mixture rises. At farther rise of the nitrogen fraction in Ar-N_2 mixtures the electron temperature fast increases and reaches rather high temperature 10 eV in pure nitrogen as it is shown in Fig. 13b. Existence of so high a temperature in the low-pressure glow discharge is questionable, especially bearing in mind that the band intensities decrease with reducing Ar fraction in the mixture. As it follows from the Langmuir probe measurements (see Fig. 6) the electron density has a minimum at N_2 fraction of about 8% N_2 (92% Ar) and the electron temperature is at maximum. When the N_2 fraction in the mixture rises to 50%, the electron density increases while the electron temperature slightly decreases. Thus, the behavior of the electron temperature derived by the intensity ratio conflicts with the Langmuir probe measurement.

When estimating the electron temperature from the intensity ratio of $I_{N_2^+,391}/I_{N_2,337}$, the authors assumed the populations of the $N_2(C^3\Pi_u, \nu = 0)$ and $N_2^+(B^2\Sigma_u^+, \nu = 0)$ excited states are mainly determined by the process of direct electron-impact excitation from the ground state of nitrogen and that their depopulation occurs due to spontaneous radiative decay. Estimations show that at the electron temperature of 1–2 eV and low pressures (~25 mTorr) of nitrogen with small addition of argon, the population mechanism is roughly valid for $N_2(C^3\Pi_u, \nu = 0)$ and $N_2^+(B^2\Sigma_u^+, \nu = 0)$ excited states. However, when the argon fraction in the Ar-N_2 mixture increases, other population mechanisms can have some influence on the populations of $N_2(C^3\Pi_u, \nu = 0)$ and $N_2^+(B^2\Sigma_u^+, \nu = 0)$ states. In addition, at the low electron temperature of 0.2–0.3 eV in the LPGD, rates of the direct electron-impact excitation of the $N_2(C^3\Pi_u, \nu = 0)$ and $N_2^+(B^2\Sigma_u^+, \nu = 0)$ excited states are so low that other population mechanisms can become more effective.

Isola et al. [58] studied the negative glow of a pulsed Ar–N_2 discharge at a pressure of 2.5 Torr for different mixture concentrations. They found that in Ar–N_2 mixtures, collisions of N_2 molecules with

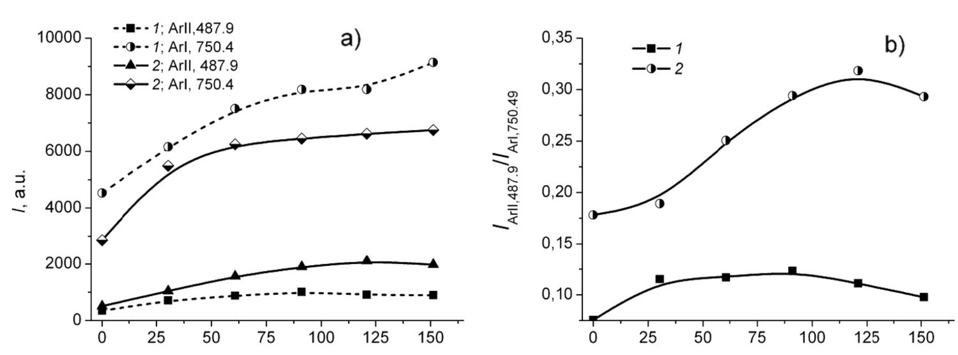

Fig. 11. Intensities (a) and intensity ratio (b) of ArII 487.98 nm and ArI 750.49 nm lines in the glow discharge in longitudinal magnetic field as a function of the magnetic field at argon pressures of 30 (*1*) and 40 mTorr (*2*); cathode voltage *U* is 1000 V.

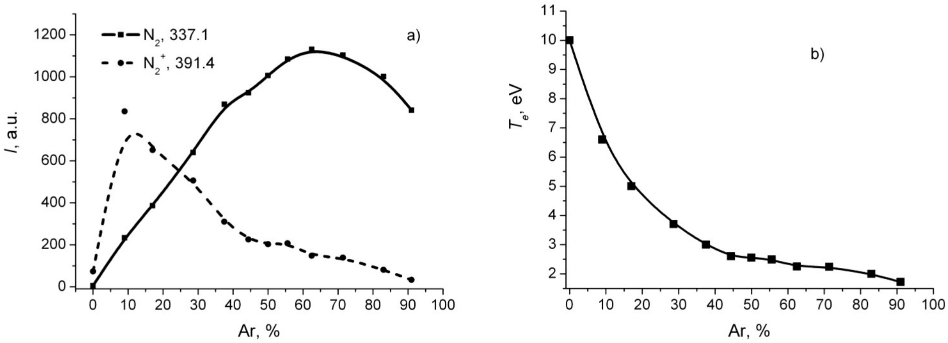

Fig. 13. Head intensities of the (0–0) band of the N_2 SPS and (0–0) band of the N_2^+ FNS (a) and the electron temperature (b) for the low-pressure glow discharge in Ar-N_2 mixture as functions of the Ar fraction in the mixture. The discharge voltage is 1000 V and the pressure is 25 mTorr.

metastable argon atoms (Ar_m^*) play a great role in the population of $N_2(C^3\Pi_u, \nu = 0{,}1)$ states (Eq. (24)).

$$Ar(^3P_{2,0}) + N_2(X, 0) \rightarrow N_2(C, v') + Ar(^1S_0), \quad k = 2.9 \times 10^{-11} \text{ cm}^3 \text{ s}^{-1} \tag{24}$$

It is shown that only when the N_2 concentration is >75% the electron collision population process is dominant. At lower N_2 concentrations, the main population process is the collision with $Ar(^3P_{2,0})$ metastable atoms [56]. The influence of the reaction (24) on $N_2(C^3\Pi_u, \nu = 0)$ is also shown in [59,60]. If the excitation transfer to N_2 from $Ar(^3P_{2,0})$ metastable atoms is high, OES methods based on spectral band head ratios cannot be directly applied to Ar–N_2 gas mixtures [61].

The pressure in a low-pressure glow discharge is roughly 100 times less than in the pulsed Ar–N_2 discharge [58]. Nevertheless, the reaction (24) can contribute to the $N_2(C^3\Pi_u)$ population. Furthermore, the growth of intensity of the 337.1 nm band when Ar concentrations are up to ~70% can be because the excitations transfer from $Ar(^3P_{2,0})$ which propagates with increasing argon concentration in the mixtures [62,63].

Kang et al. [62] calculated the relative production rate of $N_2(C^3\Pi_u)$ excited molecules through electron impact excitation ($e + N_2(X) \rightarrow N_2^*(C) + e$), metastable-metastable excitation ($N_2(A) + N_2(A) \rightarrow N_2(C^3\Pi_u)$), and excitation transfer to N_2 from $Ar(^3P_{2,0})$ metastable atoms (Eq. (24)) in an Ar–N_2 inductively coupled plasma (ICP) discharge at pressures between 20 and 200 mTorr. It is shown that at 20 mTorr, roughly 95% of $N_2(C^3\Pi_u)$ excited molecules are produced through electron impact excitation with any argon content in Ar-N_2 mixtures. At the same time with pressures of 200 mTorr, $N_2(C^3\Pi_u)$ excited molecules produced through electron impact excitation varied with a range of 40–70%. Thus, one can expect at pressures of 25 mTorr, the uncertainty of the $N_2(C^3\Pi_u)$ population caused by their production through excitation transfer is not higher than 5–10%. This uncertainty of the $N_2(C^3\Pi_u)$ population cannot lead to a great uncertainty in electron temperature so that it can reach so high values as 10 eV in pure nitrogen.

It should be remembered that simple Langmuir probe measurements show low electron temperatures of ~0.2–0.3 eV. Using double differentiation of the Langmuir probe *I-V* characteristics allows one to observe two population groups of electrons in the EEDF: the main group of 'thermalized' electrons exhibits a mean electron energy of ~0.3–0.4 eV and the second small group of "energetic" electrons exhibits a mean electron energy of ~1.0–2.5 eV. The low temperature of main group of electrons leads to great lowering rate of the direct ionization of N_2 by electron impact especially as well as excitation rate of high electronic states of N_2 molecules such as $N_2(C^3\Pi_u)$. At the same time excitation rates of low electronic states of N_2 molecules such as $N_2(A^3\Pi_u, v)$, $N_2(a'^1\Sigma_g^-, v)$, $N_2(B^3\Pi_g, v)$ states are barely reduced and remain high enough. Our estimations show that when an electron temperature is lower than 1 eV with any Ar-N_2 mixture composition rate of the direct ionization of N_2, especially when in the excited state $N_2^+(B^2\Sigma_u^+, \nu = 0)$, is low and the main mechanism of N_2 ionization most likely becomes Penning and associative ionization [64]:

$$\begin{aligned} N_2(A, v) + N_2(a', v) &\rightarrow N_2^+ + N_2 + e \\ &\rightarrow N_4^+ + e \end{aligned} \tag{25}$$

and

$$\begin{aligned} N_2(a', v) + N_2(a', v) &\rightarrow N_2^+ + N_2 + e \\ &\rightarrow N_4^+ + e. \end{aligned} \tag{26}$$

With an increase of the N_2 fraction in the mixture the electron temperature as it follows from Langmuir probe measurements decreases and all these effects become more perceptible. Therefore, assumptions of the intensity ratio $I_{N_2^+,391}/I_{N_2,337}$ method are most likely violated in the LPGD and hence it can lead to electron temperature measurement error. It is should note, that Zhu at al. also found that assumption of the electron impact excitation, which used in the OES line ratio method, is not valid in the low-pressure pure nitrogen plasma [36].

Fig. 14 shows the intensities of spectral lines NI 868.0 nm and ArI 852.1 nm in spectra of the glow discharge and the N_2 dissociation degree as a function of the Ar fraction in Ar-N_2 mixtures. The intensity of the spectral line ArI 852.1 nm increases when Ar fraction in the mixture grows. The intensity of the spectral line NI 868.0 nm reaches maximum at about 10% Ar in the mixture.

Because of the low pressure in the glow discharge probabilities of reactions between heavy particles are small relative to electron impact reactions. Therefore, the atomic nitrogen species are most likely produced by electron-impact processes such as, collisions between electrons and nitrogen molecules or between electrons and N_2^+ ions, which strongly depend on the electron temperature [65]. The dependence of the NI line intensity on Ar fraction in Ar-N_2 mixtures is similar to the dependence of intensity of the (0–0) band of the N_2^+ FNS. This suggests that at small Ar fraction in Ar-N_2 mixtures the collisions between electrons and N_2^+ ions $e + N_2^+ \rightarrow 2N$ contribute to nitrogen dissociation much more in comparison with the collisions between electrons and nitrogen molecules $e + N_2 \rightarrow 2N$. The N_2 dissociation degree decreases quickly with argon fraction in Ar-N_2 mixtures, however, when the Ar fraction reaches 40%, the rate of decrease slows down. The quick decreasing of the N_2 dissociation degree when Ar concentration in Ar-N_2 mixtures grows is mainly caused by reduction in N_2^+ density.

The N_2 dissociation degree in low-pressure gas discharges in Ar-N_2 mixtures was studied by a few experimental and theoretical researchers [17,18,62,63]. Bogaerts studied nitrogen addition to the argon glow discharge using a developed hybrid Monte Carlo–Fluid model [63]. Calculations were performed for a Grimm-type glow discharge cell (4 mm diameter and 1 cm length) at a discharge voltage of 800 V, current of 15 mA, pressure of 850 Pa (6.4 Torr) and N_2 concentrations between 0.1 and 10%. She found that the N atom density increases a bit less

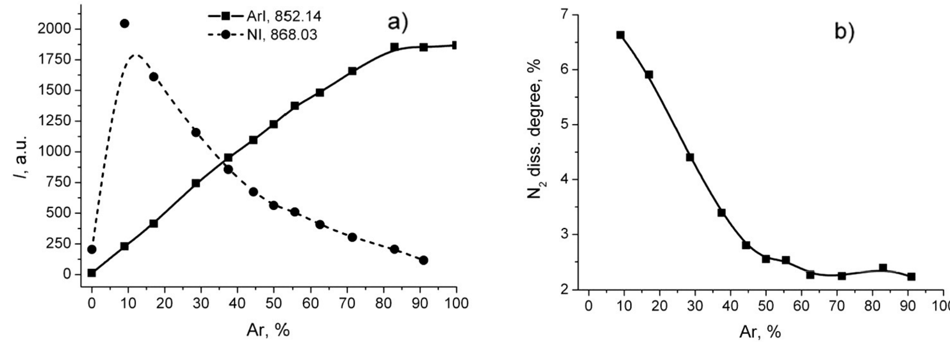

Fig. 14. Intensities of spectral lines NI and ArI (a) and the N_2 dissociation degree (b) for the low-pressure glow discharge in Ar-N_2 mixture as functions of the Ar percentage in the mixture. The discharge voltage is 1000 V and the pressure is 25 mTorr.

than linearly upon N_2 addition; thereby, giving a rise to a dissociation degree which decreases slightly for higher N_2 additions. The dissociation degree of N_2 was found on the order of 1.4–1.5% for Ar/N_2 gas mixtures up to 1% N_2, but the degree drops to a value of about 0.85% for higher N_2 additions (~10%). It was also shown that the dissociation of N_2 upon collision with Ar_m^* metastable atoms is the main production process for the N atoms. The lower dissociation degree and the slightly less than linear increase of the N atom density upon N_2 addition in the gas mixture is the cause for the drop in the Ar_m^* metastable argon atoms density. This mechanism of the nitrogen dissociation is different from the dissociation by predominantly direct electron impact with N_2^+ ions as was shown above in this section. The mechanism can be explained by the large difference in probabilities of reactions between heavy particles versus electron impact reactions at low pressure discharges ($p < 50$ mTorr) studied in this work as compared with the moderate pressure discharge conditions ($p > 1$ Torr) studied in [63].

Song et al. [17] examined the effect of argon content in an Ar-N_2 gas mixture in the range of 5%–80% in the low-pressure inductively coupled plasmas by using optical emission spectroscopy under the conditions of pressures in the range of 1–30 mTorr and applied RF powers of 200–600 W. They found the nitrogen atom density reaches a maximum at an Ar content of 30% and decreases afterwards. The dissociation fraction increases from 0.0385 at an Ar content of 5% to 0.523 at an Ar content of 80%. The increase in N_2 dissociation fraction was connected with the increase in the density of Ar metastable species ($1s_5$ and $1s_3$ levels in Pashen's notations) which interact with nitrogen molecules through a resonant energy transfer called Penning excitation. The resulting reactions of excited nitrogen molecules can dissociate to form two nitrogen atoms.

The authors [17] suggested another contribution to N-atom production is the charge exchange between nitrogen molecules and argon followed by a dissociative recombination. The power of the dc glow discharge is much less (tens of watts) than the power of the inductively coupled plasma (ICP) thus, the density of electrons is also much less. In addition the electron temperature in the LPGD is low ~0.2–0.3 eV. As a consequence, the density of the Ar metastable species in the glow discharge is less populous. These factors promote the nitrogen dissociation by predominantly direct electron impacts with N_2^+ ions and N_2 molecules in the low-pressure glow discharge.

Kang et al. [62] both experimentally and theoretically studied the dissociation of nitrogen molecules in Ar–N_2 ICP discharge at low pressure 20–200 mTorr at a constant RF power of 200 W. The measured electron temperature was almost constant, while electron density increased as a function of Ar fraction. They concluded that the dissociation of N_2 molecules in the Ar-N_2 mixed discharge occurs mainly by the electron impact dissociation at low pressures (20 mTorr), while at high pressures, the dissociative recombination is enhanced by a charge transfer between Ar^+ and $N_2(X)$, as well as the metastable-metastable pooling dissociation due to high $N_2(A^3\Sigma_u^+)$ density caused by excitation transfer between Ar_m^* and $N_2(X)$. Their conclusion confirms our estimations of the small contribution of the charge/excitation transport in N production in the low-pressure glow discharge. In the ICP [62], at pressures of 20 mTorr, the dissociation fraction of N_2 increases with Ar content in Ar-N_2 mixtures from 5% in pure nitrogen to about 10% in argon with small N_2 admixtures because the increase in electron density (1.5×10^{11}–5×10^{11} cm^{-3}) and about constant electron temperature (~3 eV). In the low-pressure glow discharges, the electron temperature is low and nitrogen dissociation occurs most likely by electron impact dissociation of N_2^+ ions and N_2 molecules. The reduction of N_2^+ density with the argon fraction in Ar-N_2 mixtures results in a decrease of N production due to the electron impact and a decrease of the nitrogen dissociation degree.

Thus, the dissociation degree and N production processes are very dependent on the kind of discharge and operating conditions, the most important of which being the Ar fraction and gas pressure. At high pressures, the charge/excitation transfer between Ar^+/Ar_m^* and N_2 are highly influenced on the production process of N atoms in Ar-N_2 mixtures. In this case, the N_2 dissociation degree increases with Ar fraction in Ar-N_2 mixtures. However, at low pressures such as 20–25 mTorr, the role of the charge/excitation transfer in the production of N atoms decreases and they occur mainly by the electron impact dissociation. The dissociation degree at low gas pressures vary in a wide range from several percent to several tens of percent.

6. Conclusions

The large area plane–symmetric low-pressure DC glow discharge in pure argon and in Ar-N_2 mixtures was studied. The low-pressure DC glow discharge is a complicated subject and the Langmuir probe, hairpin probe, and OES characterization methods were applied to obtain reliable information regarding discharge parameters and physical processes in the discharge. The data collected by OES reveal the intensities of the discharge emission spectra are weak and comprise of ArI, ArII and NI lines and N_2 and N_2^+ bands. Intensities of the lines and bands strongly depend on discharge conditions such as gas composition, pressure, magnetic field and discharge voltage. Electron density, n_e, measured by the hairpin probe is in good agreement with n_e derived from the intensity ratio of N_2 2nd positive system bands. Data from Langmuir probe analysis provide slightly higher electron density values than those collected from the hairpin probe and OES. Increasing the discharge voltage leads to higher electron density. Furthermore, when the discharge voltage increases from 700 to 1000 V at a constant pressure of 25 mTorr, the electron density grows from $1 \cdot 10^7$ cm^{-3} to $2 \cdot 10^9$ cm^{-3}. Increasing the gas pressure also increases the electron density, e.g. when the gas pressure increases from 20 to 50 mTorr, at a constant discharge voltage of 1000 V, the electron density increases from $1 \cdot 10^8$ cm^{-3} to $4 \cdot 10^{10}$ cm^{-3}.

The concept of electron temperature can be applied to the low-pressure glow discharge description with some reservations. The intensity ratio of (0–0) vibrational bands of N_2 1st negative and 2nd positive systems $I_{391.4}/I_{337.1}$ shows an electron temperature of ~1.5–3 eV and higher, depending on gas pressure and discharge voltage. Routine processing of electron temperature data deriving from Langmuir probe *I-V* characteristics provide a range of T_e ~ 0.3–0.4 eV. In-depth analysis of the EEDF using the second derivative of the Langmuir probe *I-V* characteristics shows that the EEDF is non-Maxwellian in the low-pressure glow discharge. The EEDF has two populations of electrons: the main cold bell-shape non-Maxwellian population with a mean electron energy of ~0.3–0.4 eV and the second small Maxwellian population of "hot" electrons with a mean electron energy ~ 1.0–2.5 eV. Estimations show that at electron temperature lower than 1 eV the rate of the direct electron impact ionization of N_2 is low and the main mechanism of N_2 ionization most likely becomes Penning and associative ionization. In this case, assumptions of the intensity ratio $I_{N_2^+,391}/I_{N_2,337}$ method are violated.

In the glow discharge, N_2 dissociation degree reaches about 7% at an argon fraction in the Ar-N_2 mixture < 10% and decreases afterwards approaching to ~1–2% when the argon fraction in the mixture becomes 90% and higher. In the low-pressure DC glow discharge in Ar-N_2 mixtures, N atoms are produced mainly by the electron impact processes such as, collisions between electrons and nitrogen molecules or between electrons and N_2^+ ions. At small Ar fraction in Ar-N_2 mixtures the atomic nitrogen species is most likely produced by the collisions between electrons and N_2^+ ions.

Acknowledgments

The authors are very grateful to Dr. S. Pancheshnyi, Dr. V. M. Donnelly and Dr. Yi-Kang Pu for their useful discussions and to Jeff Opal for his help with the experimental work.

Appendix A

Tables of atomic and molecular constants used in the OES methods are summarized in Tables A1–A4.

Table A1
Life time τ_0 of $N_2(C^3\Pi_u,\nu=0)$ and $N_2^+(B^2\Sigma_u^+,\nu=0)$ states and probabilities of the (0–0) vibrational transition A_{vib}(0–0) at $N_2(C^3\Pi_u,\nu')\rightarrow N_2(B^3\Pi_g,\nu'')$ and $N_2(B^2\Sigma_u^+,\nu')\rightarrow N_2(X^2\Sigma_g^+,\nu'')$ transitions [34].

Species	$N_2(C^3\Pi_u,\nu=0)$	$N_2(B^2\Sigma_u^+,\nu=0)$
τ_0, ns	42	62
A_{vib}(0–0)	0.523	0.718

Table A2
Nitrogen band parameters [37].

Transition	v'–v''	λ, nm	$q_{v'v''}$
N_2, 2nd PS	0–2	380.49	0.145
N_2, 2nd PS	1–3	375.54	0.202

Table A3
Parameters of ArI and ArII lines selected for calculating the Ar ionization degree [40,41].

Element	λ, nm	Transition	E_k, eV	E_i, eV	g_k	g_i	A_{ki}, s^{-1}	τ_k, s	f_{ik}
ArII	487.98	$4p^2D^0_{5/2}\rightarrow 4s^2P_{3/2}$	19.68	17.14	6	4	$0.823\cdot 10^8$	$0.94\cdot 10^{-8}$	0.44
ArI	750.49	$2p_1\rightarrow 1s_2$	13.479	11.828	1	3	$0.472\cdot 10^8$	$19.5\cdot 10^{-9}$	0.13

Table A4
Constants of ArI and NI spectral lines [41,46–49].

Element	Wavelength, nm	E_i, eV	E_k, eV	g_i	g_k	A_{ki}, 10^7 s^{-1}	f_{ik}	τ, ns	Level i	Level k
ArI	852.14	11.828	13.283	3	3	1.39	0.16	29	$1s_2$	$2p_4$
NI	862.92	10.690	12.126	4	4	2.66	0.297	31.73	$3s^2P$	$3p^2P^0$
NI	868.028	10.336	11.76	6	8	246	0.37	40.65	$3s^4P$	$3p^4D^0$

References

[1] A. Bogaerts, E. Neyts, R. Gijbels, J. van der Mullen, Gas discharge plasmas and their applications, Spectrochim. Acta B 57 (2002) 609–658.
[2] M.A. Lieberman, A.J. Lichtenberg, Principles of Plasma Discharges and Materials Processing, John Wiley, New York, 1994.
[3] Y.P. Raizer, Gas Discharge Physics, Springer, Berlin, New York, 1997.
[4] P.M. Chen, L. Talbot, K.J. Touryan, Electric Probes in Stationary and Flowing Plasmas: Theory and Application, Springer-Verlag, New York, 1975.
[5] N. Hershkowitz, How Langmuir probes work, in: O. Auciello, D.L. Flamm (Eds.), Plasma Diagnostics, Academic Press, Boston, 1989 (ch. 3).
[6] R.L. Stenzel, Microwave resonator probe for localized density measurements in weakly magnetized plasmas, Rev. Sci. Instrum. 47 (1976) 603–607.
[7] P.B. Piejak, V.A. Godyak, P. Garner, B.M. Alexandrovich, N.J. Sternberg, The hairpin resonator: a plasma density measuring technique revisited, Appl. Phys. 95 (2004) 3785–3791.
[8] M.A. Heald, C.B. Wharton, Plasma Diagnostics with Microwaves (Wiley Series in Plasma Physics), John Wiley & Sons Inc., London, New York, 1965 452.
[9] J.W. Coburn, E. Kay, Plasma diagnostics of an RF sputtering glow discharge, Appl. Phys. Lett. 18 (1971) 435–438.
[10] S.M. Rossnagel, K.L. Saenger, Optical emission in magnetrons: nonlinear aspects, J. Vac. Sci. Technol. A 7 (1989) 968–971.
[11] T. Mehdi, P.B. Legrand, J.P. Dauchot, M. Wautelet, M. Hecq, Optical emission diagnostics of an RF magnetron sputtering discharge, Spectrochim. Acta 48B (1993) 1023–1033.
[12] Z.J. Radzimski, O.E. Hankins, J. Cuomo, W.P. Posadowski, S. Shingubara, Optical emission spectroscopy of high density metal plasma formed during magnetron sputtering, J. Vac. Sci. Technol. B. 15 (1997) 202–208.
[13] F. Debal, M. Wautelet, J. Bretagne, J.P. Dauchotand, M. Hecq, Spatially-resolved spectroscopic optical emission of dc-magnetron sputtering discharges in argon-nitrogen gas mixtures, Plasma Sources Sci. Technol. 9 (2000) 152–160.
[14] X. Tang, D.M. Manos, Optical emission studies and neutral stream characterization of a surface reflection materials processing source, J. Vac. Sci. Technol. A 18 (2000) 1359–1365.
[15] C. Christou, Z.H. Barber, Ionization of sputtered material in a planar magnetron discharge, J. Vac. Sci. Technol. A 18 (2000) 2897–2907.

[16] D. Grondona, H. Kelly, M. Pelloni, F.O. Minotti, Spectroscopic measurements in a titanium vacuum arc with different ambient gases, Braz. J. Phys. 34 (2004) 1527–1530.
[17] M.A. Song, Y.W. Lee, T.H. Chung, Characterization of an inductively coupled nitrogen-argon plasma by Langmuir probe combined with optical emission spectroscopy, Phys. Plasmas 18 (2011) 023504.
[18] Y.W. Lee, H.-L. Lee, T.H. Chung, Dissociation fraction in low-pressure inductively coupled N_2-Ar and O_2-Ar plasmas, Curr. Appl. Phys. 11 (2011) S187–S191.
[19] X.M. Zhu, Y.K. Pu, Optical emission spectroscopy in low-temperature plasmas containing argon and nitrogen: determination of the electron temperature and density by the line-ratio method. Topical review, J. Phys. D. Appl. Phys. 43 (2010) 403001.
[20] V.M. Donnelly, Plasma electron temperatures and electron energy distributions measured by trace rare gases optical emission spectroscopy. Topical review, J. Phys. D. Appl. Phys. 37 (2004) R217–R236.
[21] D.I. Slovetsky, Mechanisms of chemical reactions in non-equilibrium fluorine-containing plasma, in: B.M. Smirnov (Ed.), Plasma Chemistry, Energoatomizdat, Moscow 1983, p. 112.
[22] R. d'Agostino, F. Cramarossa, S. de Benedictis, F. Ferraro, On the use of actinometric emission spectroscopy in C_{F6}-$_{O2}$ radiofrequency discharges: theoretical and experimental analysis, Plasma Chem. Plasma Process. 5 (1985) 239–253.
[23] V.M. Lelevkin, D.K. Otorbaev, D.C. Schram, Physics of Non-equilibrium Plasmas, Elsevier, Amsterdam, 1992.
[24] S.V. Avtaeva, D.K. Otorbaev, Diagnostics of plasma parameters in RF discharge in CF_3Br during etching of semiconductors, J. Phys. D. Appl. Phys. 26 (1993) 2148–2153.
[25] S.V. Avtaeva, M.Z. Mamytbekov, D.K. Otorbaev, Diagnostics of magnetically enhanced RF discharges in methane, argon and methane-argon mixtures, J. Phys. D. Appl. Phys. 30 (1997) 3000–3007.
[26] http://www.comsol.com.
[27] http://www.oceanoptics.com.
[28] V.I. Demidov, N.B. Kolokolov, A.A. Kydryavtsev, Probe Methods of Examination of the Low-temperature Plasma, Energoatomizdat, Moscow, 1996.
[29] E.V. Shun'ko, I-V characteristics of a cylindrical probe in a plasma with electron flow, Phys. Lett. A 147 (1990) 37–42.
[30] E.V. Shun'ko, Langmir Probe in Theory and Practice, 243, Universal Publishers, Boca Raton, Fl., USA, 2009.
[31] G.S. Gogna, S.K. Karkari, D. Boilson, M.M. Turner, Theory and application of hairpin probe in strongly magnetized plasma37th EPS Conf. on Plasma Physics, Dublin, Ireland, 2010 (P5.109).
[32] P. Paris, M. Aints, F. Valk, T. Plank, A. Haljaste, K.V. Kozlov, H.-E. Wagner, Intensity ratio of spectral bands of nitrogen as a measure of electric field strength in plasmas, J. Phys. D. Appl. Phys. 38 (2005) 3894–3899.
[33] S.V. Pancheshnyi, S.M. Starikovskaia, A.Y. Starikovskii, Population of nitrogen molecule electron states and structure of the fast ionization wave, J. Phys. D. Appl. Phys. 32 (1999) 2219–2227.
[34] S. Pancheshnyi, Comments on intensity ratio of spectral bands of nitrogen as a measure of electric field strength in plasmas, J. Phys. D. Appl. Phys. 39 (2006) 1708–1710.
[35] Y. Itikawa, Cross sections for electron collisions with nitrogen molecules, J. Phys. Chem. Ref. Data 35 (2006) 31–53.
[36] X.M. Zhu, Y.K. Pu, Using OES to determine electron temperature and density in low-pressure nitrogen and argon plasmas, Plasma Sources Sci. Technol. 17 (2008) 024002.
[37] R.N. Zare, E.O. Larsson, B.A. Berg, Frank-Condon factors for electronic band systems of molecular nitrogen, J. Mol. Spectrosc. 15 (1965) 117–139.
[38] W.R. Bennett Jr., G.N. Mercer, P.J. Kindlmann, B. Wexler, H. Hyman, Direct electron excitation cross sections pertinent to the argon ion lasers, Phys. Rev. Lett. 17 (1966) 987–991.
[39] H.R. Griem, Plasma Spectroscopy, McGraw-Hill Inc., New York, 1964.
[40] NIST, Atomic Spectral Database, http://physics.nist.gov/AtData/main_asd.
[41] P.F. Gruzdev, Transition Probabilities and Radiative Life Times of Levels of Atoms and Ions, Energoatomizdat, Moscow, 1990.
[42] H. van Regemorter, Rate of collisional excitation in stellar atmospheres, Astrophys. J. 132 (1962) 906–915.
[43] L.A. Vainshtain, I.I. Sobelman, E.A. Yukov, Excitation of Atoms and Broadening of Spectral Lines, Nauka, Moscow, 1979.
[44] G.G. Raju, Electron-atom collision cross section in argon: an analysis and comments, IEEE Trans. Dielectr. Electr. Insul. 11 (2004) 649–673.
[45] J.T. Gudmundsson, Electron Excitation Rate Coefficients for the Nitrogen Discharge, Science Institute University of Iceland, Reykjavik, Iceland, 2005 (Rep. # RH-09-2005).
[46] J.E. Sansonetti, W.C. Martin, S.L. Young, Handbook of Basic Atomic Spectroscopic Data, http://physics.nist.gov/PhysRefData/Handbook/index.html NIST, Gaithersburg, MD, 2005.
[47] A.N. Zaidel', V.K. Prokof'ev, S.M. Rayskiy, V.A. Slavnyi, E.Y. Shreider, Tables of Spectral Lines, Nauka, Moscow, 1977.
[48] G.A. Martin, J.R. Fuhr, W.L. Wiese, Atomic transition probabilities scandium through manganese, J. Phys. Chem. Ref. Data 17 (Suppl 3) (1988).
[49] A.A. Radtsig, B.M. Smirnov, Handbook on Atomic and Molecular Physics, Atomizdat, Moscow, 1978.
[50] Z. Sternovsky, S. Robertson, Langmuir probe interpretation for plasmas with secondary electrons from the wall, Physics of Plasmas 11 (2004) 3610–3615.
[51] G. Gamez, A. Bogaerts, F. Andrade, G.M. Hieftje, Fundamental studies on a planar-cathode direct current glow discharge. Part I: characterization via laser scattering techniques, Spectrochim. Acta B 59 (2004) 435–447.
[52] A. Bogaerts, R. Gijbels, G. Gamez, G.M. Hieftje, Fundamental studies on a planar-cathode direct current glow discharge. Part II: numerical modeling and comparison with laser scattering experiments, Spectrochim. Acta B 59 (2004) 449–460.
[53] A. Garscadden, K.G. Emeleus, Notes on the effect of noise on Langmuir probe characteristics, Proc. Phys. Soc. 79 (1962) 535–541.
[54] V.I. Kolobov, Striations in rare gas plasmas, J. Phys. D. Appl. Phys. 39 (2006) R487–R506.
[55] J.M. Anderson, Ultimate and secondary electron energies in the negative glow of a cold-cathode discharge in helium, J. Appl. Phys. 31 (1960) 89–94.
[56] W. Stern, Grid-probe measurements in a negative glow, Beitr. Plasmaphys. 9 (1969) 59–73.
[57] A. Bogaerts, A. Quentmeier, N. Jakubowski, R. Gijbels, Plasma diagnostics of an analytical Grimm-type glow discharge in argon and in neon: Langmuir probe and optical emission spectrometry measurements, Spectrochim. Acta Part B. 50 (1995) 1337–1349.
[58] L. Isola, M. López, B.J. Gómez, Study of the excitation mechanisms of the second positive system in the negative glow of a N_2–Ar discharge, J. Phys. D. Appl. Phys. 44 (2011) 375204.
[59] C. Foissac, J. Krištof, A. Annušová, V. Martišovitš, P. Veisand, P. Supiot, Vacuum UV and UV spectroscopy of a N_2–Ar mixture discharge created by an RF helical coupling device, Plasma Sources Sci. Technol. 19 (2010) 055006.
[60] C. Foissac, J. Krištof, A. Annušová, P. Veisand, P. Supiot, Spectroscopic diagnostics and modelling of a N_2–Ar mixture discharge created by an RF helical coupling device: I. Kinetics of $N_2(B^3\Pi_g)$ and $N_2(C^3\Pi_u)$ states, Plasma Sources Sci. Technol. 21 (2012) 055021.
[61] N. Britun, M. Gaillard, A. Ricard, Y.M. Kim, K.S. Kim, J.G. Han, Determination of the vibrational, rotational and electron temperatures in N_2 and Ar–N_2rf discharge, J. Phys. D. Appl. Phys. 40 (2007) 1022–1029.
[62] N. Kang, F. Gaboriau, S. Ohand, A. Ricard, Modeling and experimental study of molecular nitrogen dissociation in an Ar–N2 ICP discharge, Plasma Sources Sci. Technol. 20 (2011) 045015.
[63] A. Bogaerts, Hybrid Monte Carlo - fluid model for studying the effects of nitrogen addition to argon glow discharges, Spectrochim. Acta B 64 (2009) 126–140.
[64] V. Guerra, P.A. Sá, J. Loureiro, Kinetic modeling of low-pressure nitrogen discharges and post-discharges, Eur. Phys. J. Appl. Phys. 28 (2004) 125–152.
[65] N. Itagakia, S. Iwataa, K. Mutaa, A. Yonesub, S. Kawakamic, N. Ishiid, Y. Kawaia, Electron-temperature dependence of nitrogen dissociation in 915 MHz ECR plasma, Thin Solid Films 435 (2003) 259–263.